PERFORMANCE-BASED APPROACH TO ASSESS DURABILITY OF REACTIVE POWDER CONCRETE

A Dissertation

by

UMUT BAKHBERGEN

BEng, MSc in Civil Engineering

Submitted in fulfilment of the requirements for the degree of

DOCTOR OF PHILOSOPHY

in Science, Engineering and Technology

Supervisors:

Chang-Seon Shon, Ph.D.

Dichuan Zhang, Ph.D.

Jong R. Kim, Ph.D.

Jenny Liu, Ph.D., P.E.

School of Engineering and Digital Sciences

Nazarbayev University

August 2022

Author’s declarations

DECLARATION

I hereby, declare that this manuscript, entitled “PERFORMANCE-BASED APPROACH TO ASSESS DURABILITY OF REACTIVE POWDER CONCRETE”, is the result of my own work except for quotations and citations which have been duly acknowledged.

I also declare that, to the best of my knowledge and belief, it has not been previously or concurrently submitted, in whole or in part, for any other degree or diploma at Nazarbayev University or any other national or international institution.

Name: Umut Bakhbergen Date: December 15, 2022

1 Abstract

Claiming that a relatively new type of concrete called reactive powder concrete (RPC) is reported to have superior compressive and tensile strength, and potentially improved durability because of dense microstructure, it is suggested as a material for the pile foundation system where renewable energy is to be stored in the form of compressed air inside the hollow section of the pile. Even though strength and microstructure of RPC are studied extensively by number of researchers, and some studies focus on the external sulfate attack and freezing and thawing resistance of the material, modeling of its durability properties is barely attempted. Hence, the main aims of this research are to verify the strength and properties of RPC before the exposure to damaging environments, as well as to evaluate its behavior under the effect of sulfate and freezing and thawing damages. In addition, it is suggested that the performance of RPC under external sulfate attack and freezing and thawing damage can be predicted by comprehensive models. Thus, the objective of this research is to extend the existing knowledge of the RPC performance under different exposure conditions by studying its characteristics while varying its mixture contents, and to develop simple performance-based assessment tools to evaluate characteristics of the material.

The initial part of the research focuses on the verification of strength and microstructure of RPC without steel fibers in the mixtures made from locally available materials. Response surface methodology and partial factorial design of experiments were used to develop testing program that varied two important RPC mixture design parameters: water-to-binder ratio and silica fume content. Material testing included compressive and flexural strength, and shrinkage when samples are cured in normal and warm temperatures. Preliminary investigation of the ESA durability was performed to understand the mechanism of the attack and gain a minimal knowledge on the extent of RPC's improved durability features. Moreover, aggregate packing degree was corrected by application of Toufar model which was also verified experimentally.

The main part of the research consisted of the two distinct components, namely experimental investigation and performance-based assessment model development for external sulfate attack and freezing and thawing resistance. The

results obtained in the previous part were incorporated to develop a new testing

program that included RPC mixtures with steel fiber addition. Aiming to minimize the experimental effort, Taguchi design of experiments was used to determine the optimal RPC mixture with beneficial characteristics against external sulfate attack and freezing and thawing damage. Experimental variables are: steel fiber content, water-to-binder ratio, and silica fume content for both sulfate attack and freezing and thawing resistance. Furthermore, exposure conditions such as concentration and temperature of the solution, as well as exposure mode (cyclic or continuous) were included as influence factors in the design of experiments for external sulfate attack testing.

Hence, comprehensive analysis of the results obtained in both parts of the research allow to state that RPC has superior strength, microstructural and durability properties. In addition, data obtained in the main part of the research on RPC mixtures exposed to external sulfate attack and freezing and thawing damage was used to develop performance-based models. In case of external sulfate attack, modeling was based on the expansion behavior of the material, namely, it was used to calculate the reaction rate constant and activation energy for the sulfate attack reaction. Thus, activation energy was used as a single variable to assess the sulfate exposure performance of RPC. Moreover, it was used to determine the threshold value of activation energy which is suggested as the minimal energy barrier that needs to be overcome to initiate the sulfate induced damage in RPC. In case of freezing and thawing damage, number of characteristics that included both initial properties and damage induced changes were employed to obtain the single value of frost resistance number which is suggested to be used instead of classical durability factor that reflects only obtained freezing and thawing damage.

Accordingly, this research has not only experimentally verified the strength, improved microstructure, and durability of RPC, but yielded two performance-based models that could be used to assess the external sulfate attack and freezing and thawing resistance of RPC. In addition to extensive experimental data and analysis that allows in-depth understanding of RPC properties, it provides with several distinct mixture design that are likely to perform exceptionally for various demanding applications.

Acknowledgements

Firstly, I would like to express my gratitude towards my supervisors Professor Chang Shon and Professor Dichuan Zhang. It has been their supervision and directions throughout the duration of my research which has allowed me to successfully complete the PhD research. I am also appreciative for advises and support from my co-supervisors, Professor Jong Kim and Professor Jenny Liu, and from faculty and staff of the School of Engineering and Digital Sciences and Nazarbayev University.

This research was supported by "Development of a Renewable Energy Storage System using Reinforced Concrete Foundations" project, funded by Nazarbayev University.

I sincerely thank laboratory assistants, managers and students of the School of Engineering and Digital Sciences. My sincere thanks to Eldar Sharafutdinov, Islam Mukhammedrakhym, Kirill Kryzhanovskii, Islam Orynbassarov and Ayazhan Bazarbekova who provided expertise and assistance to this research. I also express my gratitude towards laboratory assistants of the Core Facilities of Nazarbayev University for sharing laboratory and providing resources for the experimental part of the research.

I would like to express my special thanks to my husband and daughter and other members of my family for providing me with exclusive support and understanding for the duration of PhD research.

1 Table of Contents

2 Author's declarations .....i 3
Abstract .....ii 4
Acknowledgements.....iv 5
Table of Contents ..... v 6
List of Tables.....ix 7
List of Figures .....xi 8
Acronyms and Definitions.....xvii 9
Dedication xviii
10 1. Introduction 1 11
1.1 Problem statement. .....2 12 1.2 Hypothesis, aims and objectives.....4 13 1.3 Organization of the dissertation.....6 14 2. Literature review ..... 7 15 2.1 Reactive powder concrete: material properties.....7 16 2.1.1 Components.....8 17 2.1.2 Hydration and microstructure.....10 18 2.1.3 Fresh properties.....12 19 2.1.4 Hardened properties .....12 20 2.2 Reactive powder concrete: mechanical properties .....14 21 2.2.1 Compressive strength .....14 22 2.2.2 Tensile strength .....15 23 2.2.3 Shrinkage.....16 24 2.3 Reactive powder concrete: durability properties.....18 25 2.3.1 External sulfate attack .....18 26 2.3.2 Freezing and thawing damage.....23 27 2.4 Modeling ESA .....25 28 2.5 Modeling FT.....29 29 3. Materials and Methods..... 31 30 3.1 Materials and Sample Preparation .....31 31 3.1.1 Binders.....31 32 3.1.2 Aggregate .....32 33 3.1.3 Supplements 32

34 3.1.4 Mixing procedure and sample preparation.....33 35 3.2 Testing program.....35 36 3.2.1 Aggregate properties .....35 37 3.2.2 RPC fresh properties .....38 38 3.2.3 RPC hardened properties.....40 39 3.2.4 RPC strength tests .....43 40 3.2.5 RPC durability tests.....44 41 3.2.6 RPC microstructural properties.....45 42 3.3 Design of experiments.....47 43 3.3.1 Fractional factorial method .....48 44 3.3.2 Response surface method .....48 45 3.3.3 Taguchi method.....48 46 3.4 Experimental setup .....50 47 3.4.1 RSM based mixture proportioning .....50 48 3.4.2 Partial factorial DoE mix proportioning.....51 49 3.4.3 Mixture proportioning for packing degree study .....52 50 3.4.4 Taguchi DoE mixture proportioning .....53 51 4. Mixture proportion and characterization of RPC..... 54 52 4.1 Optimization of RPC mixture design by response surface method.....54 53 4.1.1 Fresh properties of RPC .....55 54 4.1.2 Hardened properties of RPC.....58 55 4.1.3 Drying shrinkage of RPC .....63 56 4.1.4 Optimization of RPC mix design component.....67 57 4.1.5 Analyzing test results in comparison to analytical simulations .....68 58 4.1.6 Summary .....69 59 4.2 Assessment of RPC subject to ESA.....71 60 4.2.1 Compressive strength of RPC subject to ESA .....71 61 4.2.2 Expansion and mass gain of RPC subject to ESA.....77 62 4.2.3 Microstructural properties of RPC subject to ESA .....80 63 4.2.4 Summary .....85 64 4.3 Statistical Analysis of ESA in RPC.....87 65 4.3.1 Analysis of variance .....87 66 4.3.2 Taguchi analysis.....88 67 4.3.3 Summary 89

68 4.4 Effect of aggregate packing on RPC strength.....91 69 4.4.1 Aggregate packing model.....92 70 4.4.2 Properties of sand and blends.....93 71 4.4.3 Simulation and experimental verification .....94 72 4.4.4 Workability and compressive strength .....96 73 4.4.5 Summary .....98 74 5. Evaluation of external sulfate attack resistance of RPC..... 99 75 5.1 Experimental analysis of ESA resistance of RPC .....99 76 5.1.1 Initial properties .....100 77 5.1.2 Ultrasonic pulse velocity (UPV) .....116 78 5.1.3 Compressive strength .....122 79 5.1.4 Specific gravity.....133
80 5.1.5 Correlating UPV, compressive strength and specific gravity of RPC mixtures142 81
82 5.1.6 Modulus of rupture.....145 83 5.1.7 Dielectric constant.....154 84 5.1.8 Length change .....162 85 5.1.9 Mass change .....171 86 5.1.10 Correlating length and mass change of RPC mixtures.....178 87 5.1.11 Visual and microstructural analysis .....181 88 5.1.12 Summary .....187 89 5.2 Modeling ESA in RPC.....190 90 5.2.1 Development of ESA model.....190
91 5.2.2 Evaluation of performance of RPC through ESA model determined characteristics.....195 92
93 5.2.3 Summary .....206 94 6. Evaluation of freezing and thawing resistance of RPC..... 208 95 6.1 Experimental analysis of FT resistance of RPC .....208 96 6.1.1 Initial properties .....210 97 6.1.2 Length change .....218 98 6.1.3 Mass change .....220 99 6.1.4 Correlating length and mass change.....222 100 6.1.5 Modulus of rupture.....223

101 6.1.6 Relative dynamic modulus of elasticity (RDME) and Durability Factor 102 (DF) 226

103 6.1.7 Summary 229 104 6.2

Modeling FT in RPC 231 105 6.2.1

Development of FT model 232 106 6.2.2

Evaluation of FT performance of RPC through FRN .....234 107 6.2.3 Summary

.....235 108 7.

Conclusion..... 237

109 7.1 Assessment of ESA and FT resistance of RPC through performance-based 110 model defined parameters 237

111 7.2 Limitations and recommendations for future study.....243 112 8.

Glossary..... 245 113 9.

References ..... 247 114 10.

Bibliography..... 269 115 11.

Appendices..... 291 116

Appendix A 291 117

Appendix B.....293

List of Tables

Table 2.1. UHPC hydration chemistry terms. 10
Table 3.1. Properties of binders..... 31
Table 3.1. Properties of binders (cont.)..... 32
Table 3.2. Properties of fine aggregate..... 32
Table 3.3. Sodium sulfate solution concentration guide. 33
Table 3.4. Determination of number of experiments. 49
Table 3.6.CCD RSM applied for RPC. 50
Table 3.7. Mixture proportioning of RPC designed by CCD RSM. 51
Table 3.8. Mixture proportion of RPC. 52
Table 3.9. Properties of each sand fraction. 52
Table 3.10. Mixture Proportioning of RPC mixtures..... 53
Table 4.1. Experimental setup for RPC mixture optimization. 54
Table 4.1. Experimental setup for RPC mixture optimization (cont.). 55
Table 4.2. Flowability of RPC mixtures..... 55
Table 4.3. Compressive strength and porosity of RPC mixtures. 59

Table 4.4. Density, porosity, and P/D of six key RPC mixtures.....61 18
Table 4.5. Summary of RSM analysis.....68 19
Table 4.6. Experimental setup for assessment of RPC subject to ESA.....71 20
Table 4.7. MIP porosities of RPC mixtures. 84 21
Table 4.8. Variable levels in experimental program. 87 22
Table 4.9. ANOVA results. 87 23
Table 4.9. ANOVA results (cont.). 88 24
Table 4.10. Taguchi analysis results. 88 25
Table 4.11. Experimental setup for packing degree effect on RPC properties. 92 26
Table 4.12. Properties of sand fractions. 94 27
Table 4.13. Workability and 7-day compressive strength test results.....96 28
Table 4.13. Workability and 7-day compressive strength test results (cont.). 97 29
Table 5.1. Experimental setup for evaluation of ESA resistance of RPC. 99 30
Table 5.2. Workability of RPC mixtures.....101
31 Table 5.3. Rating of RPC mixtures based on compressive strength and specific gravity.
32 143
33 Table 5.3 (cont.). Rating of RPC mixtures based on compressive strength and specific
34 gravity.....144

35 Table 5.4. Rating of RPC mixtures based on length and mass change. 179 36
Table 5.4 (cont.). Rating of RPC mixtures based on length and mass change.....180 37
Table 6.1. Experimental setup for evaluation of FT resistance of RPC.....208 38
Table 6.2. Apparent specific gravity of RPC mixtures. 213 39
Table 6.3. FT damage level of RPC mixtures. 223 40
Table 6.4. Variables for FRN. 232 41
Table 6.5. Final variable for FRN calculation.....233 Table
A-1. R^2
42 for polynomial fit of length change data (ESA).....291 43 Table A-2.
Model calculated k and L_0 values. .....291 Table B-1. R^2
44 values of polynomial fit for length change data (FT).....293 45 Table B-2.
Code calculated length change data. 293

List of Figures

Fig. 1.1. Schematic view of CAES incorporated into pile foundation system [1]. 1

Fig. 1.2. Loading condition of the hollow pile foundation system: (a) side view; (b) top view [1]. 2

Fig. 1.3. Research tasks. 4

Fig. 2.1. Basic components and proportioning of RPC.....8

Fig. 3.1. Mixing procedure for RPC.....33

Fig. 3.2. Moisture conditions of fine aggregate. 36

Fig. 3.3. RPC development process. 47

Fig. 4.1. Relative flowability of six key mixtures.....56

Fig. 4.2. Penetration resistance of RPC: (a) effect of SF content; (b) effect of w/b. .57

Fig. 4.3. Setting time of RPC: (a) effect of SF content; (b) effect of w/b. 57 13

Fig. 4.4. Relative flowability vs. setting time of RPC mixtures.....58

14 Fig. 4.5. Effect of SF content on compressive strength of RPC: (a) 23±2 °C; (b) 40±2 15 °C.....60

16 Fig. 4.6. Effect of SF content on flexural strength of RPC: (a) 23±2 °C; (b) 40±2 °C. 17 61

18 Fig. 4.7. Effect of w/b compressive strength of RPC: (a) 23±2 °C; (b) 40±2 °C. 62

19 Fig. 4.8. Effect of SF content on flexural strength of RPC: (a) 23±2 °C; (b) 40±2 °C. 20 63

21 Fig. 4.9. Effect of SF content on drying shrinkage of 1-day cured RPC samples.....64

22 Fig. 4.10. Effect of SF content on drying shrinkage of 7-day cured RPC samples: (a) 23 23±2 °C; (b) 40±2 °C.....65

24 Fig. 4.11. Effect of w/b on drying shrinkage of 1-day cured RPC samples.....66

25 Fig. 4.12. Effect of w/b on drying shrinkage of 7-day cured RPC samples: (a) 23±2 °C; 26 (b) 40±2 °C. 66

27 Fig. 4.13. Contour plots for combined effect of w/b and SF on compressive strength 28 of RPC: (a) 7-day; (b) 28-day; (c) 56-day.....67

29 Fig. 4.14. Analytical simulations and laboratory test results comparison.....69 30

Fig. 4.15. 1-day compressive strength of RPC mixtures.....72

31 Fig. 4.16. Early age compressive strength development: (a) 0.35M Na_2SO_4; (b) 0.7M 32 Na_2SO_4; (c) 1.4M Na_2SO_4.....72

33 Fig. 4.17. Effect of SF content on early age compressive strength: (a) 0.35M Na_2SO_4; 34 (b) 0.7M Na_2SO_4; (c) 1.4M Na_2SO_4.....73

35 Fig. 4.18. Effect of w/b on early age compressive strength: (a) 0.35M Na_2SO_4; (b) 36 0.7M Na_2SO_4; (c) 1.4M Na_2SO_4. 74

37 Fig. 4.19. Compressive strength development: (a) 0.35M Na_2SO_4; (b) 0.7M Na_2SO_4; 38 (c) 1.4M Na_2SO_4.....75

39 Fig. 4.20. Effect of SF content on compressive strength development: (a) 0.35M 40 Na_2SO_4; (b) 0.7M Na_2SO_4; (c) 1.4M Na_2SO_4. 76

41 Fig. 4.21. Effect of w/b on compressive strength development: (a) 0.35M Na_2SO_4; (b) 42 0.7M Na_2SO_4; (c) 1.4M Na_2SO_4. 77

43 Fig. 4.22. Length change of RPC mixtures: (a) 0.35M Na_2SO_4; (b) 0.7M Na_2SO_4; (c) 44 1.4M Na_2SO_4.....78

45 Fig. 4.23. Mass change of RPC mixtures: (a) 0.35M Na_2SO_4; (b) 0.7M Na_2SO_4; (c) 46 1.4M Na_2SO_4.....79

47 Fig. 4.24. SEM micrographs of RPC mixtures: (a) 1.4M – 0.22WB-15SF, mag.: 8.87K; 48 (b) 0.7M – 0.26WB-20SF, mag.: 3.27K; (c) 0.35M – 0.22WB-0SF, mag.: 1.6K. 81

49 Fig. 4.25. XRD patterns of RPC mixtures: (a) 0.35M – 0.22WB-25SF; (b) 0.7M – 50
0.22WB-15SF; (c) 1.4M – 0.18WB-20SF. 82

51 Fig. 4.26. Pore distribution of RPC mixtures: (a) 0.35M Na_2SO_4; (b) 0.7M Na_2SO_4; (c)
52 1.4M Na_2SO_4.....83

53 Fig. 4.27. Initial porosity and sorptivity of RPC mixtures: (a) effect of w/b; (b) effect 54
of SF content. 85

55 Fig. 4.28. Sieve analysis of river sand.....93 56

Fig. 4.29. Toufar model calculation of sand packing degree. 95 57

Fig. 4.30. Experimented and calculated packing degrees. 96 58

Fig. 5.1. Experimental program for ESA resistance of RPC.....100 59

Fig. 5.2. Relative flowability of RPC mixtures.....101

60 Fig. 5.3. Effect of mixture design parameters on relative flowability of RPC: (a) steel 61
fiber content; (b) w/b; (c) SF content. 102

62 Fig. 5.4. Volume of permeable voids of RPC mixtures. 104

63 Fig. 5.5. Effect of mixture design parameters on volume of permeable voids of RPC: 64
(a) steel fiber content; (b) w/b; (c) SF content. 105

65 Fig. 5.6. Rate of water absorption of RPC mixtures: (a) initial; (b) secondary. 106

66 Fig. 5.7. Effect of mixture design parameters on initial sorptivity of RPC: (a) steel fiber
67 content; (b) w/b; (c) SF content.....107

68 Fig. 5.8. Effect of mixture design parameters on secondary sorptivity of RPC: (a) steel
69 fiber content; (b) w/b; (c) SF content. 107

70 Fig. 5.9. 1-day UPV of RPC mixtures.....108

71 Fig. 5.10. Effect of mixture design parameters on 1-day UPV of RPC: (a) steel fiber 72
content; (b) w/b; (c) SF content.....109

73 Fig. 5.11. 1-day compressive strength of RPC mixtures.....110

74 Fig. 5.12. Effect of mixture design parameters on 1-day compressive strength of RPC:
75 (a) steel fiber content; (b) w/b; (c) SF content. 111

76 Fig. 5.13. 1-day specific gravity of RPC mixtures.....112

77 Fig. 5.14. Effect of mixture design parameters on 1-day specific gravity of RPC: (a) 78
steel fiber content; (b) w/b; (c) SF content.....112

79 Fig. 5.15. 1-day modulus of rupture of RPC mixtures.....113

80 Fig. 5.16. Effect of mixture design parameters on 1-day modulus of rupture of RPC: 81
(a) steel fiber content; (b) w/b; (c) SF content. 114

82 Fig. 5.17. 1-day dielectric constant of RPC mixtures. 115

83 Fig. 5.18. Effect of mixture design parameters on 1-day dielectric constant of RPC: (a)
84 steel fiber content; (b) w/b; (c) SF content.....116

85 Fig. 5.19. Early age UPV of RPC mixtures: (a) 20 ºC; (b) 40 ºC; (c) 60 ºC.....117

86 Fig. 5.20. UPV of RPC at continuous exposure at 20 ºC, effect of: (a) steel fiber 87
content; (b) w/b; (c) SF content; (d) Na_2SO_4 concentration.....119

88 Fig. 5.21. UPV of RPC at continuous exposure at 40 ºC, effect of: (a) steel fiber 89
content; (b) w/b; (c) SF content; (d) Na_2SO_4 concentration.....120

90 Fig. 5.22. UPV of RPC at continuous exposure at 60 ºC, effect of: (a) steel fiber 91
content; (b) w/b; (c) SF content; (d) Na_2SO_4 concentration.....121

92 Fig. 5.23. Early age compressive strength of RPC mixtures: (a) cyclic exposure; (b) 20
93 ºC; (c) 40 ºC; (d) 60 ºC.....123

94 Fig. 5.24. Later age compressive strength of RPC mixtures: (a) cyclic exposure; (b) 20
95 ºC; (c) 40 ºC; (d) 60 ºC.....125

96 Fig. 5.25. Compressive strength of RPC at cyclic exposure at 20 ºC, effect of: (a) steel
97 fiber content; (b) w/b; (c) SF content; (d) Na_2SO_4 concentration. 127

98 Fig. 5.26. Compressive strength of RPC at continuous exposure at 20 ºC, effect of: (a)
99 steel fiber content; (b) w/b; (c) SF content; (d) Na_2SO_4 concentration.....129

100 Fig. 5.27. Compressive strength of RPC at continuous exposure at 40 ºC, effect of: (a)
101 steel fiber content; (b) w/b; (c) SF content; (d) Na_2SO_4 concentration.....130

102 Fig. 5.28. Compressive strength of RPC at continuous exposure at 60 ºC, effect of: (a)
103 steel fiber content; (b) w/b; (c) SF content; (d) Na_2SO_4 concentration.....132

104 Fig. 5.29. Early age specific gravity of RPC mixtures: (a) cyclic exposure; (b) 20 ºC;
105 (c) 40 ºC; (d) 60 ºC.....134

106 Fig. 5.30. Later age specific gravity of RPC mixtures: (a) cyclic exposure; (b) 20 ºC;
107 (c) 40 ºC; (d) 60 ºC.....135

108 Fig. 5.31. Specific gravity of RPC at cyclic exposure at 20 ºC, effect of: (a) steel fiber
109 content; (b) w/b; (c) SF content; (d) Na_2SO_4 concentration.....137

110 Fig. 5.32. Specific gravity of RPC at continuous exposure at 20 ºC, effect of: (a) steel
111 fiber content; (b) w/b; (c) SF content; (d) Na_2SO_4 concentration. 138

112 Fig. 5.33. Specific gravity of RPC at continuous exposure at 40 ºC, effect of: (a) steel
113 fiber content; (b) w/b; (c) SF content; (d) Na_2SO_4 concentration. 140

114 Fig. 5.34. Specific gravity of RPC at continuous exposure at 60 ºC, effect of: (a) steel
115 fiber content; (b) w/b; (c) SF content; (d) Na_2SO_4 concentration. 141

116 Fig. 5.35. Final rating of RPC mixtures on compressive strength and specific gravity:
117 (a) based on rating value; (b) based on mix design.....145

118 Fig. 5.36. Early age modulus of rupture of RPC mixtures: (a) cyclic exposure; (b) 20
119 ºC; (c) 40 ºC; (d) 60 ºC.....146

120 Fig. 5.37. Later age modulus of rupture of RPC mixtures: (a) cyclic exposure; (b) 20
121 ºC; (c) 40 ºC; (d) 60 ºC.....147

122 Fig. 5.38. Modulus of rupture of RPC at cyclic exposure at 20 ºC, effect of: (a) steel 123
fiber content; (b) w/b; (c) SF content; (d) Na_2SO_4 concentration. 149

124 Fig. 5.39. Modulus of rupture of RPC at continuous exposure at 20 ºC, effect of: (a) 125
steel fiber content; (b) w/b; (c) SF content; (d) Na_2SO_4 concentration.....150

126 Fig. 5.40. Modulus of rupture of RPC at continuous exposure at 40 ºC, effect of: (a) 127
steel fiber content; (b) w/b; (c) SF content; (d) Na_2SO_4 concentration.....152

128 Fig. 5.41. Modulus of rupture of RPC at continuous exposure at 60 ºC, effect of: (a) 129
steel fiber content; (b) w/b; (c) SF content; (d) Na_2SO_4 concentration.....153

130 Fig. 5.42. Dielectric constant of RPC mixtures: (a) cyclic exposure; (b) 20 ºC; (c) 40
131 ºC; (d) 60 ºC. 155

132 Fig. 5.43. Dielectric constant of RPC at cyclic exposure at 20 ºC, effect of: (a) steel 133
fiber content; (b) w/b; (c) SF content; (d) Na_2SO_4 concentration. 157

134 Fig. 5.44. Dielectric constant of RPC at continuous exposure at 20 ºC, effect of: (a) 135
steel fiber content; (b) w/b; (c) SF content; (d) Na_2SO_4 concentration.....158

136 Fig. 5.45. Dielectric constant of RPC at continuous exposure at 40 ºC, effect of: (a) 137
steel fiber content; (b) w/b; (c) SF content; (d) Na_2SO_4 concentration.....160

138 Fig. 5.46. Dielectric constant of RPC at continuous exposure at 60 ºC, effect of: (a) 139
steel fiber content; (b) w/b; (c) SF content; (d) Na_2SO_4 concentration.....161

140 Fig. 5.47. Length change of RPC mixtures: (a) cyclic exposure; (b) 20 ºC; (c) 40 ºC; 141
(d) 60 ºC. 163

142 Fig. 5.48. Length change of RPC at cyclic exposure at 20 ºC, effect of: (a) steel fiber
143 content; (b) w/b; (c) SF content; (d) Na_2SO_4 concentration.....166

144 Fig. 5.49. Length change of RPC at continuous exposure at 20 ºC, effect of: (a) steel 145
fiber content; (b) w/b; (c) SF content; (d) Na_2SO_4 concentration. 167

146 Fig. 5.50. Length change of RPC at continuous exposure at 40 ºC, effect of: (a) steel 147
fiber content; (b) w/b; (c) SF content; (d) Na_2SO_4 concentration. 168

148 Fig. 5.51. Length change of RPC at continuous exposure at 60 ºC, effect of: (a) steel 149
fiber content; (b) w/b; (c) SF content; (d) Na_2SO_4 concentration. 170

150 Fig. 5.52. Mass change of RPC mixtures: (a) cyclic exposure; (b) 20 ºC; (c) 40 ºC; (d)
151 60 ºC. 172

152 Fig. 5.53. Mass change of RPC at cyclic exposure at 20 ºC, effect of: (a) steel fiber 153
content; (b) w/b; (c) SF content; (d) Na_2SO_4 concentration.....173

154 Fig. 5.54. Mass change of RPC at continuous exposure at 20 ºC, effect of: (a) steel 155
fiber content; (b) w/b; (c) SF content; (d) Na_2SO_4 concentration. 174

156 Fig. 5.55. Mass change of RPC at continuous exposure at 40 ºC, effect of: (a) steel 157
fiber content; (b) w/b; (c) SF content; (d) Na_2SO_4 concentration. 176

158 Fig. 5.56. Mass change of RPC at continuous exposure at 60 ºC, effect of: (a) steel 159

fiber content; (b) w/b; (c) SF content; (d) Na_2SO_4 concentration. 177

160 Fig. 5.57. Final rating of RPC mixtures on length and mass change: (a) based on rating 161 value; (b) based on mix design.....180

162 Fig. 5.58. RPC compressive strength samples exposed to ESA: (a) cyclic; (b) 20 ºC; 163 (c) 40 ºC; (d) 60 ºC.....182

164 Fig. 5.59. RPC modulus of rupture samples exposed to ESA: (a) cyclic; (b) 20 ºC; (c) 165 40 ºC; (d) 60 ºC. 182

166 Fig. 5.60. RPC length/mass change samples exposed to ESA: (a) cyclic; (b) 20 ºC; (c) 167 40 ºC; (d) 60 ºC. 183

168 Fig. 5.61. SEM images with EDS spectrum of RPC samples exposed to ESA: (a) 169 cyclic; (b) 20 ºC; (c) 40 ºC; (d) 60 ºC.....184

170 Fig. 5.62. XRD analysis results of RPC samples exposed to ESA: (a) cyclic; (b) 20 ºC; 171 (c) 40 ºC; (d) 60 ºC.....186

172 Fig. 5.63. Flow chart of the model development.....190

173 Fig. 5.64. Polynomial fitting of length change data. 191

174 Fig. 5.65. Linear fitting of polynomial length change versus time data.....192

175 Fig. 5.66. Activation energy determination.....193

176 Fig. 5.67. Threshold value determination.....194

Fig. 5.68. Reaction rate constant: (a) 1st stage; (b) 2nd 177 stage; (c) k_{total}.....196

178 Fig. 5.69. Correlating reaction rate constants to sorptivity of RPC. 197

179 Fig. 5.70. Reaction rate constant of RPC mixtures, effect of: (a) steel fiber content; (b) 180 w/b; (c) SF content; (d) Na_2SO_4 concentration. 199

Fig. 5.71. Ultimate expansion: (a) 1st stage; (b) 2nd 181 stage; (c) total.....200

182 Fig. 5.72. Ultimate expansion of RPC mixtures, effect of: (a) steel fiber content; (b) 183 w/b; (c) SF content; (d) Na_2SO_4 concentration. 202

184 Fig. 5.73. Activation energy.....204

185 Fig. 5.74. Correlating activation energy to volume of permeable voids in RPC. 204

186 Fig. 5.75. Activation energy of RPC mixtures, effect of: (a) steel fiber content; (b) w/b; 187 (c) SF content; (d) Na_2SO_4 concentration. 205

188 Fig. 6.1. Experimental program for FT resistance of RPC.....209

189 Fig. 6.2. FT cycle arrangement: (a) 16 cycles; (b) 1 cycle.....210

190 Fig. 6.3. Absorption of RPC mixtures: (a) after immersion; (b) after immersion and 191 boiling.....211

192 Fig. 6.4. Effect of mixture design parameters on absorption of RPC mixtures: (a) after 193 immersion, steel fiber content; (b) after immersion, w/b; (c) after immersion, SF 194 content; (d) after immersion and boiling, steel fiber content; (e) after immersion and 195

boiling, w/b; (a) after immersion and boiling, SF content. 212

196 Fig. 6.5. Effect of mixture design parameters on apparent SG of RPC: (a) steel fiber 197 content; (b) w/b; (c) SF content.....214

198 Fig. 6.6. 14-day cylindrical compressive strength of RPC mixtures.....215

199 Fig. 6.7. Effect of mixture design parameters on 14-day cylindrical compressive 200 strength of RPC: (a) steel fiber content; (b) w/b; (c) SF content. 216

201 Fig. 6.8. 14-day modulus of rupture (MoR) of RPC mixtures. 217

202 Fig. 6.9. Effect of mixture design parameters on 14-day modulus of rupture of RPC: 203 (a) steel fiber content; (b) w/b; (c) SF content. 217

204 Fig. 6.10. Length change of RPC mixtures subject to FT cycles. 219

205 Fig. 6.11. Effect of mixture design parameters on length change of RPC after 300 FT 206 cycles: (a) steel fiber content; (b) w/b; (c) SF content. 219

207 Fig. 6.12. Mass change of RPC mixtures subject to FT cycles.....221

208 Fig. 6.13. Effect of mixture design parameters on mass change of RPC after 300 FT 209 cycles: (a) steel fiber content; (b) w/b; (c) SF content. 221

210 Fig. 6.14. Length versus mass change of RPC mixtures subject to FT cycles.....222

211 Fig. 6.15. Modulus of rupture (MoR) of RPC mixtures after 300 FT cycles.....223

212 Fig. 6.16. Effect of mixture design parameters on modulus of rupture of RPC mixtures 213 after 300 FT cycles: (a) steel fiber content; (b) w/b; (c) SF content. 224

214 Fig. 6.17. Change of MoR of RPC mixtures after 300 FT cycles. 225

215 Fig. 6.18. Effect of mixture design parameters on ΔMoR of RPC mixtures: (a) steel 216 fiber content; (b) w/b; (c) SF content. 226

217 Fig. 6.19. RDME of RPC mixtures subject to FT cycles. 227

218 Fig. 6.20. DF of RPC.....228

219 Fig. 6.21. Effect of mixture design parameters on DF of RPC mixtures: (a) steel fiber 220 content; (b) w/b; (c) SF content.....228

221 Fig. 6.22. Parameters used to develop FRN. 231

222 Fig. 6.23. FRN of RPC mixtures. 234

223 Fig. 6.24. Effect of mixture design parameters on FRN of RPC mixtures: (a) steel fiber; 224 (b) w/b; (c) SF content.....235

225

1 Acronyms and Definitions

CAES	Compressed Air Energy Storage
CH	Calcium Hydrate

CSH	Calcium Silicate Hydrate
DF	Durability Factor
ESA	External sulfate attack
E_a	Activation Energy
FRN	Frost Resistance Number
FT	Freezing thawing
k	Reaction rate constant
MoR	Modulus of Rupture
OPC	Ordinary Portland Cement concrete
PV	Photovoltaic
RDME	Relative Dynamic Modulus of Elasticity
RPC	Reactive Powder Concrete
RSM	Response Surface Methedology
SCAES	Small scale compressed air energy storage
SCM	Supplementary cementitious materials
SF	Silica Fume
SP	Superplasticizer
UPV	Ultrasonic Pulse Velocity
w/b	Water-to-binder ratio

Dedication

To my grandfather Jarylkasyn, who dreamed of this day. To my grandmother Kaziza, who always wishes the best for me. To my mother Gulden, who never allows to give up. To my husband Murat, who is always by my side. To my daughter Narmina, who once will do this herself.

For their endless love, encouragement, and support.

1. Introduction

Portland cement concrete is one of the most abundant and widely used materials in construction industry. However, like any other material concrete is subject to the damaging action of environmental factors that reduce its service life and diminish properties like strength and durability. This research focuses on the properties and characterization of special type of Portland cement concrete, and its performance under damaging environmental conditions.

Claiming that a relatively new type of concrete called reactive powder concrete (RPC) is reported to have superior compressive and tensile strength, and potentially improved durability because of dense microstructure, it is suggested as a material for the pile foundation system where renewable energy is to be stored in the form of compressed air inside the hollow section of the pile. The concept is presented in Fig. 1.1 [1].

14

15 Fig. 1.1. Schematic view of CAES incorporated into pile foundation system [1].

16 The proposed arrangement results in dual functionality of pile foundation [2]. 17 Fig. 1.2 presents simplified loading conditions of hollow pile foundation system. 18 Firstly, conventional loading from superstructure load (vertical force N) and 19 surrounding soil (skin friction f, bedrock bearing force B, and small lateral pressure

20 p_0); secondly, additional tensile loading (all-around pressure p) on the inner wall of 21 the pile from highly pressurized air inside.

22

23 Fig. 1.2. Loading condition of the hollow pile foundation system: (a) side view; (b) top view [1].

24 RPC is a relatively new type of ultra-high-performance concrete first 25 developed in France, in 1994, and it is characterized by potentially high compressive 26 and tensile strength and enhanced durability properties [3]. Nevertheless, because of 27 complex loading conditions, implementation of the project is associated with several 28 issues that require sophisticated research and investigation.

29 1.1 Problem statement.

30 Implementing RPC as a material for pile foundation system with incorporated CAES 31 requires analysis and verifications of its strength and durability properties. Firstly, 32 compressed air is to be stored in the hollow section of the pile. Hence, the effective 33 area that resists superstructural load as well as the thickness of the pile itself are 34 reduced. The material with superior strength characteristics is required for the 35 application. However, properties of RPC are highly dependent on number factors 36 related to raw materials and mixture design [4-6]. Secondly, pile foundations are 37 subject to the action of environmental factors such as water table of surrounding soils, 38 chemical agents dissolved in the groundwater, and its temperature. Since the

39 monitoring of the properties and repair of damaged regions is not an option for 40

underground pile foundations with long service life improved durability of the material becomes highly important characteristic. In addition, in-situ groundwater table was reported to be relatively high [7]. Furthermore, high concentration of sulfate ions was detected in the groundwater. Hence, the problem of the external sulfate attack (ESA) which is a durability issue associated with microstructural damage, expansion, and deterioration of concrete due to chemical reaction between sulfate ions and concrete hydration products becomes an important factor for consideration [8]. Extreme continental climate with long and cold winters (the lowest temperature detected in the capital city of Kazakhstan is -52 ºC), and relatively short spring season followed by hot summers (the highest temperature detected in the capital city of Kazakhstan is +42 ºC) arises the issue of freezing and thawing of surrounding soils and associated water movement for pile foundation system [9]. Freezing and thawing cycles in concrete result in microstructural pressures that damage the internal structure of concrete resulting in the scaling and deterioration of its material properties [10, 11]. Hence, application of RPC as a material for pile foundation system with incorporated CAES is associated with strength and durability issue, namely: high compressive and tensile strength of the material is required for complex loading condition; high ESA and FT durability is required for long service life under suggested environmental conditions. Number of research have investigated the strength and microstructure of RPC. However, its durability in terms of ESA and especially FT is an ongoing topic of the research. In addition, study of the cyclic exposure to ESA in RPC as well as modeling of ESA and FT durability of RPC was not thoroughly attempted. Hence, the study aims to add on top of existing RPC properties knowledge, and most importantly intends to fill into the research gap in the fields of modeling of RPC's durability issues.

64 1.2 Hypothesis, aims and objectives

65 It is suggested that RPC has superior compressive and tensile strength, and improved 66 durability under ESA and FT damage. The performance of RPC under ESA and FT 67 damage can be predicted by comprehensive models.

68 Hence, the main aims of this research are:

69 • to verify the strength and durability of the RPC by material tests. 70 • to develop assessment models of the behavior of the RPC under ESA 71 and FT damage.

72 The objective of this research is to extend the knowledge of the RPC 73 performance under different exposure conditions by studying its characteristics while 74 varying its mixture contents, and to develop simple, but comprehensive performance 75 based assessment tools to evaluate the characteristics of different RPC mixtures. To 76 accomplish the objectives and achieve the aims of this study the research was divided 77 into several interrelated research tasks that are summarized in Fig. 1.3.

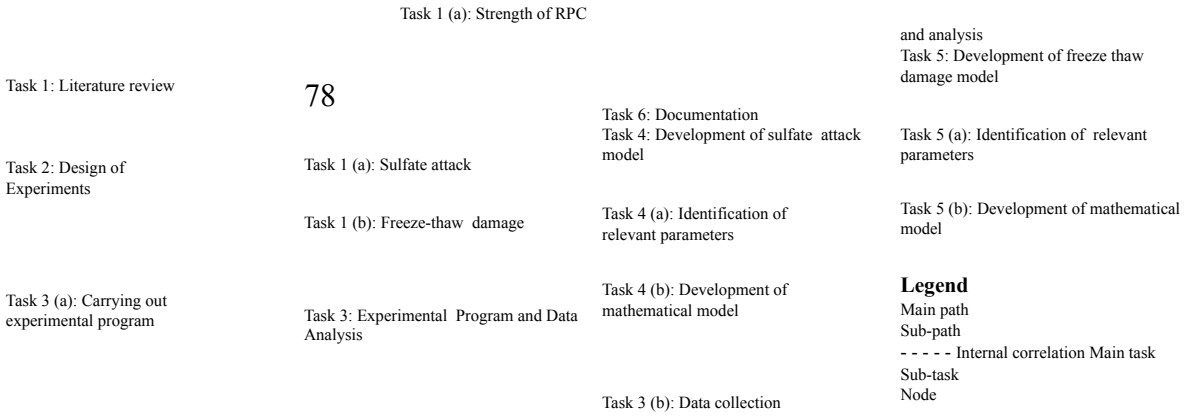

79 Fig. 1.3. Research tasks.

80 Accordingly, there are 6 main research tasks required to accomplish the 81 objectives and achieve the aims of the study:

82 1. Literature review of state-of-the-art research on the topic of RPC 83 strength and durability (ESA and FT damage).

84 2. Design of Experiments (DoE) required for verification of research 85 hypothesis.

86 3. Experimental program and data analysis is one of the main research 87 tasks since it

will not only provide the experimental data for verification of RPC 88 strength and durability properties, but also be a base for development of the 89 performance-based models.

90 4. Development of ESA model is associated with analysis of experimental 91 data, identification of relevant parameters and development of simple comprehensive 92 model. ESA durability of RPC and ESA model is the main part of the study. 93 5. Development of FT model is associated with analysis of experimental 94 data, identification of relevant parameters and development of simple comprehensive 95 model. FT durability of RPC and FT model is the supplementary part of the study. 96 6. Documentation includes the dissertational thesis which organization is 97 presented in the following section.

98 1.3 Organization of the dissertation

99 The dissertation consists of eleven chapters. Each chapter is briefly summarized 100 below.

101 Chapter 1 is an introduction that includes research statement and organization 102 of the dissertation.

103 Chapter 2 presents the review of available literature on the relevant study 104 topics. General properties, microstructure and strength of RPC are described briefly in 105 the beginning, followed by the detailed review of ESA and FT resistance of RPC, and 106 existing models of ESA and FT performance of ordinary concrete.

107 Chapter 3 is the description of materials and methods of this study. The 108 chapter starts from the materials and sample preparation information for RPC testing 109 and is followed by the description of testing method used for the study based on the 110 standard concrete testing methods. The chapter also contains the general information 111 on design of experiment techniques and experimental setup of concrete mixtures used 112 to accomplish the objectives of the study.

113 Chapter 4 presents the study on mixture proportioning and characterization 114 of RPC, including optimization of RPC mixtures strength, and assessment of its 115 behavior under ESA as well as the improvement of raw aggregate by application of 116 packing degree model.

117 Chapter 5 is the evaluation of external sulfate attack resistance of RPC 118 through experimental analysis, discussion of RPC properties under ESA, and 119 development of the model.

120 Chapter 6 is the evaluation of freezing and thawing resistance of RPC through 121 experimental analysis, discussion of RPC properties under ESA, and development of 122 the model.

123 Chapter 7 summarizes the main finding and conclusions of the study, as well 124 as provides recommendations on further development of the research. 125 Chapter 8 is the glossary of relevant terms used in the study. 126 Chapters 9 and 10 provide list of references and bibliography of the research 127 correspondingly.

128 Chapter 11 includes the appendices of the study that were not included into 129 the main body of the dissertation.

2. Literature review

Concrete was a part of construction industry since the Roman times. A Roman concrete was a material consisting of aggregates, gypsum, and quicklime, and pozzolana, and it was used in number of Roman structures [12]. However, contemporary concrete was developed only by 19th century. It has undergone major development throughout the 20th century. By the end of 20th century, a new advanced concrete: ultra-high-performance concrete (UHPC) was developed [13]. The major significance of the material is its superior properties that achieved through mixture design and curing techniques. In this chapter the properties of UHPC also called reactive powder concrete (RPC) will be described. Namely, its material and mechanical properties, as well as its durability issues including external sulfate attack (ESA) and freezing thawing (FT) resistance will be described. In addition, a review of the existing ESA and FT modeling methods for ordinary concrete is provided.

2.1 Reactive powder concrete: material properties

The RPC was first invented in France in 1994, while the Sherbrook Bridge in Canada (the first RPC structure) was constructed in 1997 [14]. RPC is defined as high strength and ductility concrete with improved physical and mechanical characteristics. These properties of RPC are achieved by elimination of coarse aggregates and improved particle packing of fine aggregate, addition of ultra-fine pozzolanic materials and fibers, and reduction of water-to-binder ratio [15]. Fig. 2.1 summarizes the composition of RPC.

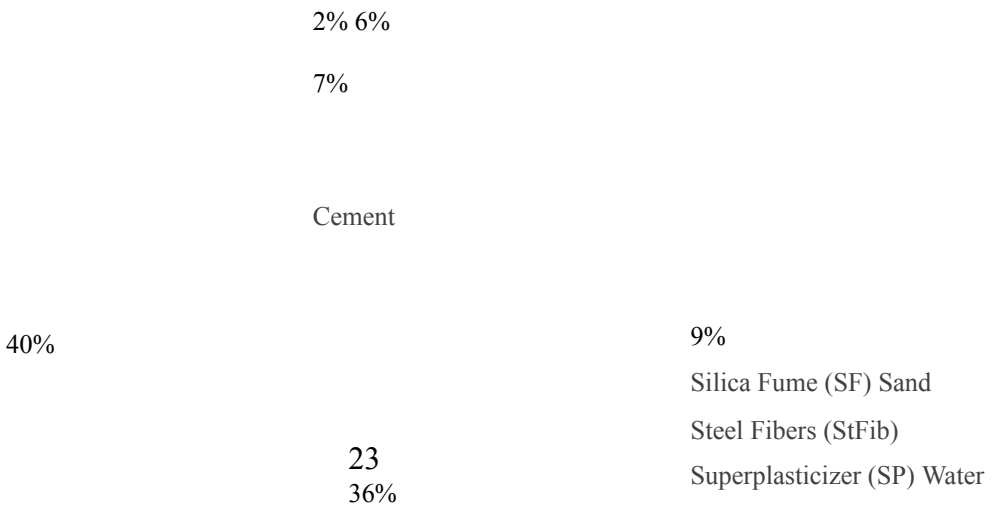

Fig. 2.1. Basic components and proportioning of RPC.

In their original research Richard and Cheyrezy introduced the RPC as the material with following characteristics [3]:

• Removal of coarse aggregate improves homogeneity of the mix. • Optimization of granular mixture enhances concrete compaction. • Concrete hydration properties are improved by addition of pozzolanic materials.

• Reduction of w/b is optimized by addition of superplasticizing components that improve workability of RPC throughout the mixing and placement.

• Enhancement of microstructure can be achieved by temperature treatment.

• Ductility is improved by addition of small size steel fibers. 2.1.1

Components

Ordinary Portland cement (OPC) is the main binding material that is used in RPC. According to Fig. 2.1 it is also one of the main constituents of the RPC. The typical size of cement particles is about 15 μm, which makes it the second largest particle size in the mixture [16]. RPC employs as much as double amount of cement

compared to OPC concrete. It is argued that portion of cement that have not been

hydrated act as a fillers of RPC microstructure still improving its properties [17]. 44 Micro silica also known as Silica Fume (SF) is a by-product material of 45 production of ferrosilicon alloys and silicon metal [15]. The average diameter of SF 46 is about 0.15 μm which makes the finest component of RPC [18]. Addition of SF 47 into RPC improves its microstructural, mechanical and durability properties [15, 48 16, 19]. In addition, the workability of RPC can also be improved since the excess 49 SF acts as a filling material which enhances flowability of fresh RPC mixes [4, 20]. 50 Various studies recommend adding SF in the amount of 20 to 30% of cement by 51 mass [3, 15, 20-22].

52 Ordinary tap water is usually used for RPC hydration in adequate 53 quantities for cement hydration [3, 23]. RPC is characterized by very low water-to 54 binder ratios (w/b). Thus, typical w/b of OPC concrete is about 0.4-0.5 [5, 23]. 55 However, an optimum w/b for RPC is reported as 0.13-0.26 [3, 5, 24, 25]. It is 56 argued that w/b is inversely proportional to concrete's compressive strength [3, 26]. 57 Water that is not employed in hydration will results in the formation of voids and 58 increase of permeability that diminishes the strength of concrete. The minimal w/b 59 in RPC was about 0.08, nevertheless, it was not able to ensure the adequate 60 workability levels [3].

61 Since low w/b of RPC results in the workability issues high range water 62 reducing admixtures or superplasticizers (SP) are added to improve its workability 63 properties [27]. According to different studies the optimal range of SP dosage is 64 0.5-2.5% [28, 29]. However, the amount of SP depends on number of mixture 65 design factors and general compatibility between them and SP itself; hence, it can

66 be varied until the desired characteristics are achieved [30, 31]. 67 Increased compressive strength and homogeneity make RPC subject to 68 ductility issues which are often addressed by addition of steel fibers [6, 32, 33]. 69 Nevertheless, the optimum amount of steel fiber addition exists beyond which 70 increase of steel fiber content will not positively affect the ductility of RPC [34]. 71 The most used steel fibers have the Ø 0.20 mm, and 13 mm length [35, 36]. A

72 recommended amount of steel fiber that improves ductile properties of RPC without

73 compromising its cost is about 1-2% of aggregate by mass [37, 38]. 74 Fine aggregate or sand is another main constituent of the RPC. The main 75 roles of fine aggregate in RPC are to enhance workability through particle gradation 76 and improve mechanical strength due to its load carrying ability [26]. The typical 77 size of fine aggregate in RPC which can be either silica sand, quartz sand or natural 78 sand ranges from 150 to 600 μm making it the largest particle in RPC mixture [15, 79 29]. In general, the failure of concrete under loading is associated with crack 80 propagation, while the initiation of microcracks takes place in the aggregate-cement 81 interface also called interfacial transition zone (ITZ) [39]. Hence, the mechanical 82 properties of RPC are improved by elimination of coarse aggregate and enhanced 83 further by improving the packing of fine aggregate [40]. Hence, limited porosity of 84 RPC achieved by improved packing of fine aggregate improves its mechanical 85 strength [41].
86 Thus, all ingredients of RPC have influence on its properties that is 87 maintained and improved by changing the amount and type of the mixture 88 constituents.

89 2.1.2 Hydration and microstructure

90 The hydration of cement and pozzolans in RPC is similar to OPC concretes. Eq. 2.1 91 and 2.2 represents simplified chemical reactions of the UHPC hydration process 92 [42]. More common representations used for concrete chemistry are given in Table 93 2.1.

94 $2C_3S + 7H_2O \rightarrow 3CH \cdot 2CSH \cdot 4H_2O + 3C(H)_2$ {2.1} 95 $CSH + C(H)_2 \rightarrow C_3S_2H_3 \cdot H_2O$ {2.2}

96 Table 2.1. UHPC hydration chemistry terms.

Chemical formula	Concrete chemistry abbreviation	Name
Ca_3SiO_5	C3S, C2S	Calcium silicate
$Ca{\cdot}2SiO_2{\cdot}4H_2O$, $CaSiO_3{\cdot}H_2O$	CSH	Calcium silicate hydrate
$3CaO{\cdot}Al_2O_3$	C3A	Tricalcium aluminate
$4CaO{\cdot}Al_2O_3{\cdot}Fe_2O_3$	C4AF	Tetra calcium alumino-ferrite

97 Hence, calcium silicates which is the main component of cement reacts 98 with water in the exothermal reaction producing CSH, which is the main strength

99 bearing phase in concrete, and calcium hydroxide, which is low strength byproduct 100 of the reaction. Pozzolanic materials like silica fume consist of silicon dioxide (up 101 to 94%) which allows them to react with cement hydration byproduct and produce

102 additional CSH [6]. CSH provides homogeneous microstructure to concrete. Thus, 103 enhancement of CSH production in UHPC results in the improved homogeneity of 104 the material. The hydration of cementitious materials (cement and SF) starts 105 immediately upon the contact with water and is believed to continue up to the age 106 of 28-days; however, it is argued that the process of hydration in UHPC can take 107 much longer time [43]. Hydration of minor components like C_3A and C_4AF result 108 in the production phases with undesired crystalline characteristics [44]. It has been 109 argued that high temperature curing enhances hydration and production of CSH in 110 concrete [45]. Thus, RPC owes its superior strength characteristics to the addition 111 of pozzolans that accelerate the cement hydration and react with hydration 112 byproduct to produce strength bearing phases.

113 Moreover, use of pozzolanic mineral admixtures in addition to design of 114 RPC mixtures to achieve high packing density and result in the material with 115 reduced porosity, specifically continuous porosity. As an illustration, it was 116 reported that discontinuity of capillary pores in RPC with w/b=0.20 was detected 117 upon 26% of cement hydration while for OPC concretes this was achieved only 118 after 56% hydration [46]. The typical pore size of UHPC is about 2-3 nm, and its 119 total porosity measured by MIP is about 2.23% [47]. In addition, the porosity of 120 UHPC decreases as hydration advances. The porosity values ranging from 5 to 9% 121 was reported for RPC mixtures with various mineral admixtures [48]. After the 122 completion of hydration process, UHPC consists of aggregate and paste matrix. As 123 it was mentioned previously, aggregate-cement interface is the weakest point of the 124 matrix. However, it was reported that RPC has highly homogeneous ITZ without 125 pores consisting mainly of CSH [49, 50]. Another important factor influencing and 126 limiting the extensive pore formation in RPC is low w/b. Thus, in RPC water is not 127 in excess, and cementitious materials that did not take part in the hydration process 128 act as pore fillers improving homogeneity of the material [5, 6].

129 Hence, the microstructural properties of RPC are dependent on the 130 hydration process. RPC has superior microstructural characteristics owing to its 131 constituents and mixture proportioning.

132 2.1.3 Fresh properties

133 Properties of RPC tend to depend on the mixing procedure. Furthermore, number 134 of important characteristics like mechanical strength or water permeability of 135 concrete can be predicted based on the concrete's fresh properties. 136 Setting time of UHPC is defined when the stiffness of the mixture reaches 137 1000 MPa [51]. Reaching this value of stiffness also indicates the onset of 138 autogenous shrinkage. However, it is also possible to differentiate the initial setting 139 time as the time of up to 15 h when the stiffness of 3.45 MPa is reached, and final 140 setting time of about 18-20 h with 27.6 MPa penetration resistance [33]. A typical 141 setting time of UHPC is between 6 to 12 h [3, 52, 53]. However, setting time of 142 RPC can be delayed due to SP addition or surface covering of RPC molds [27, 51- 143 54].

144 While considering setting time of RPC mixtures involves complex testing 145 procedure, determining its workability is more available method to evaluate the 146 fresh properties of UHPC. In general, increase in workability of concrete is 147 achieved by increasing the water content. In contrast, UHPC requires minimizing 148 w/b to achieve higher strength values. However, removing of coarse aggregates, 149 using ultrafine powders and well-graded fine aggregates as well as addition of SP 150 admixtures allows to achieve tolerable workability without compromising the 151 strength of RPC [27]. Addition of steel fibers, on the other hand, limits the 152 workability of RPC, especially for steel fibers with higher aspect ratio [55, 56]. The 153 recommended flow diameter of UHPC mixtures ranges from 200 to 350 mm [55]. 154 The adequate workability of RPC ensures ease of handling and placing the concrete.

155 2.1.4 Hardened properties

156 Porosity and permeability of concrete are important characteristics that define its 157 susceptibility to external environmental damage. Thus, as it was previously

158 mentioned, enhancement of microstructural properties of UHPC results in the 159 decreased porosity of the material (typical 1-2% of the total volume) [57, 58]. The 160 main influencing factors were defined as the w/b and elevated temperature 161 treatment

[59-61].

162 In addition, RPC shows reduced water absorption capacity which is up to 163 60 times less than in OPC concretes [59, 62, 63]. The water sorptivity coefficient of RPC is reported to be 0.044kg/m^2/$h^{0.5}$ 164 which is about 15 times lower than for 165 OPC concrete [63]. It is argued that addition of pozzolanic materials in general, and 166 of SF specifically can decrease the sorptivity of RPC [64]. In addition, the sorptivity 167 of RPC decreases with increasing its SF content which is possibly due to pore filling 168 effect of SF. Some studies suggest that increasing w/b tend to increase the sorptivity 169 of concrete since it is associated with increase of pore connectivity and permeability 170 [65]. Concrete sorptivity can also be used as a tool to evaluate its compressive 171 strength. As an illustration, an existence of tolerable correlation between sorptivity 172 of UHPC and its compressive strength was proved in the experimental study with the R^2 173 being 0.88 [64]. It is possible that sorptivity can also be correlated to 174 durability properties of RPC since it is the representative of RPC's microstructural 175 and pore space characteristics. Thus, the correlation between carbonation and sorptivity was reported to have R^2

176 =0.90 to 0.99 [64]. Hence, the properties of RPC 177 are representative of its microstructural characteristics, and interdependent.

178 2.2 Reactive powder concrete: mechanical properties

179 RPC proved itself to be a material with excellent strength characteristics including 180 both compressive and tensile strength. This chapter will review available literature 181 on the topic of RPC's compressive and tensile strength, and shrinkage behavior.

182 2.2.1 Compressive strength

183 Number of experimental investigations on RPC's mechanical properties showed it 184 as excellent construction material with high and very high compressive strength 185 (CS) [3, 66]. The main factors influencing the CS of RPC are dense packing of the 186 components, and its w/b [29]. In fact, it is argued that increasing w/b decreases the 187 compressive strength of RPC [26]. CS can also be increased by increasing SF 188 content [67]. Curing technique, namely steam curing can also improve the CS of 189 RPC [13]. This is achieved by increasing the rate of hydration in RPC [68]. 190 Employing high temperature treatment results in the enhancement of pozzolanic 191 reaction, which in turn results in the formation of additional CSH [58, 68]. 192 Formation of strong CSH structures results in the significant decrease of pore space 193 leading to improved mechanical strength [33, 68-71]. Nevertheless, the positive 194 effect of heat treatment is observable only if it is applied for relatively long period 195 of time. Thus, only 4% of difference in CS was observed between 2-day heat cured 196 and normally cured specimen [72]. In contrast, up to 40% increase of CS was 197 observed for specimen cured at 90 ºC for 28-days [73-75].

198 It was observed that addition of steel fiber has little effect on CS of RPC. 199 Nevertheless, it was argued that presence of steel fibers changes the failure mode 200 of the UHPC. RPC without steel fibers experience sudden ductile failure called 201 explosive spalling, while addition of still fibers allows the specimen to remain intact 202 without signs of spalling type failure [76]. In addition, number of investigations 203 showed that increasing steel fiber dosage in UHPC can lead to extensive formation 204 of "weak" fiber-paste interface, which can result in the decrease of its mechanical 205 strength [39, 61, 73, 75]. However, a slight increase of compressive strength is 206 observed when steel fiber content is increased up to a certain limit. Addition of steel

fibers enhance lateral strains toleration which is presumed to be the main attributing factor of increase of compressive strength upon addition of steel fibers [53, 77-80]. Number of experimental investigations proved the effect of size and shape of the specimen on compressive strength of specimen. Namely, larger specimen tends to have lower compressive strength which is possibly due to higher possibility of formation of larger size microdefects [33, 72, 81]. In addition, cubic specimens tend to show higher compressive strength compared to cylindrical specimen which is due to the confinement effect [53, 82].

The values of compressive strength reported for UHPC are about 80-120 MPa in average [27, 83, 84]. However, values as high as 150-200 MPa are also reported by number of researchers [29, 85-87]. Thus, the compressive strength of RPC is considerably higher compared to OPC concrete.

2.2.2 Tensile strength

Tensile strength of RPC is evaluated through several tests. The first test to evaluate the tensile strength is split tensile strength test. Split tensile strength value for RPC is about 10 MPa and can go as high as 20 MPa [29, 86]. There exists a correlation between tensile and compressive strength of RPC: in general, the tensile strength is considered to be 10% of compressive strength [88]. Significant difference in the tensile strength values between conventional concrete and UHPC is possibly due to improved crack capacity in tension of cement matrix as well as the fiber reinforcement in UHPC [89].

Another test employed to assess the tensile behavior of RPC is flexural strength test. The values of flexural strength for RPC range between 20 to 50 MPa [29, 84-86]. In general, the flexural strength of RPC is about 5 times higher than for OPC concrete and is about 2 times higher than its tensile strength [29]. Thus, when tensile strength of RPC is discussed in this study it refers to RPC's general tensile behavior if not clarified further as flexural or split tensile strength.

Increased tensile strength of RPC is due to its densified microstructure and addition of steel fibers [33, 90]. Steel fiber content tends to have the most dramatic effect on the tensile strength of RPC. Thus, increase of fiber content up to 2.5%

237 resulted in more than 100% increase of RPC's flexural strength [79]. Fibers in RPC
238 prevent formation and propagation of microcracks, the failure in flexural loading is
239 characterized by the formation of single vertical or close to vertical macrocrack [53,
240 78]. In addition, not only steel fiber content, but its aspect ratio and shape are stated
241 to have an effect of flexural strength of RPC [80, 91, 92]. In addition, flexural 242
strength of RPC tends to decrease with increasing the sample size for testing [91]. 243
The possible reason is the higher "wall" effect of fibers in specimen with smaller 244
size [53, 79, 93, 94]. Hence, the fiber characteristics (aspect ratio, shape, orientation 245
and content) have a significant effect on tensile strength of RPC. Increasing the 246
fiber content appears to be the effective method to achieve the required tensile 247
strength [37, 95, 96]. Nevertheless, it appears that addition of 1% of steel fiber by 248
volume fraction can initiate the strain hardening behavior in UHPC resulting in the 249
improved ductility and appropriate tensile strength [38, 77]. Thus, improved tensile 250
strength of RPC can be achieved with minimal steel fiber addition.

251 2.2.3 Shrinkage

252 Shrinkage in concrete is the result of the evaporation or any other water reduction
253 from the cement hydration process [6]. Shrinkage is the main cause of cracking in
254 cement-based materials. In general, drying shrinkage of UHPC is reported be very
255 low [97]. Thus, the highest shrinkage rate is observed during the first 14-day period.
256 14 to 100-day period UHPC are characterized by the steady increase of shrinkage
257 rate, with further reduction. Increase of w/b tends to increase the shrinkage strains
258 in UHPC. Nevertheless, the development of drying and autogenous shrinkage is 259
different in UHPC. Thus, RPC with low w/b tend to have high autogenous, but low 260
drying shrinkage. Increase of shrinkage due to increase of SCM content and 261
fineness of aggregate was observed [98]. Namely, increase of SF content tends to 262
promote the hydration process significantly influencing autogenous shrinkage in 263
RPC [99]. The autogenous shrinkage of concrete is a macroscopic change of 264
volume resulting from the hydration and chemical processes in the UHPC while the 265
drying shrinkage is a volumetric change that occurs due to evaporation or loss of 266
water (drying) process [100]. Hence, addition of SF or replacement of cement by

267 pozzolanic materials like SF tends to reduce the long-term shrinkage in UHPC. The 268 reduction of shrinkage up to 80% is possible. On the other hand, this can result in 269 the considerable reduction of early age strength [101, 102]. In addition, increasing 270 fiber content and employing high temperature curing can positively influence the 271 shrinkage behavior of RPC. However, simultaneously, it increases the relative cost 272 of material production [103, 104]. Hence, improvement of shrinkage behavior of 273 RPC can limit its other mechanical properties as well as the quality of the material.

2.3 Reactive powder concrete: durability properties

One of the major characteristics of RPC along with its high strength is its durability. Durability of concrete is defined as its ability to resists the damaging environmental actions without quality deterioration [42]. The most abundant durability issues in concrete are associated with penetration of water, attack from chemical agents, corrosion of steel reinforcement, alkali-silica reaction, freeze-thaw damage, and

carbonation [105]. Majority of durability issues can be addressed through timely maintenance, nevertheless, associated costs and accessibility of concrete structures makes durability issues significant problem [106]. Permeability and density of the matrix of concrete are the main characteristics influencing its durability properties since most durability issues are linked to the penetration of substances into the concrete microstructure [107, 108]. Decreased porosity of RPC that is due to exclusion of coarse aggregate and inclusion of pozzolanic materials like silica fume as well as low w/b significantly increases its durability compared to ordinary concrete [103, 109]. Simple water absorption coefficient of RPC can be considered as an indicator of its durability properties. Thus, increased water abruption in concrete implies increased susceptibility to durability issues. On the other hand, matrix densification through decrease of w/b improves RPC's durability properties [87, 105, 110]. In this study RPC's performance subject to two durability issues, namely, external sulfate attack and freeze-thaw damage will be considered.

2.3.1 External sulfate attack

External sulfate attack (ESA) is durability issues associated with the ingress of sulfate ions and the damaging chemical reactions in concrete microstructure. The damage upon ESA is related to the expansion, cracking, reduction of strength and stiffness, and complete failure of cementitious material [8, 111, 112]. Foundations are one of the main structures subject to the action of ESA since remedial actions and maintenance are not possible for them. It is necessary to differentiate the chemical and physical sulfate attack. Thus, the chemical sulfate attack refers to the expansion and deterioration related to the chemical reaction between sulfate ions and concrete hydration products. On the other hand, physical sulfate attack is linked

to the surface scaling due to crystallization of sulfate salts [8, 113]. The term ESA will relate to chemical sulfate attack with not specified otherwise. The development of sulfate attack is associated with several distinct processes: transport, chemical reaction, expansive forces, and mechanical response [113]. The penetration of sulfate ions into concrete microstructure are required for the initiation of ESA. Hence, the direct contact between concrete porous space and sulfate environment is

necessary for the initiation of the process. Thus, porosity and 311 permeability of concrete plays an important role in the development of sulfate 312 induced damage inn RPC. Reduction of w/b, densification of internal structure 313 through aggregate packing, as well as addition of SF make RPC pore space 314 condensed and unavailable for sulfate penetration. It was investigated that the 315 sulfate attack performance of RPC is equal or greater than the performance of 316 sulfate-resisting Portland cement concretes [114]. The presence of sulfate ions in 317 the surrounding media of concrete structures results in the shift of chemical 318 equilibrium in the system of aqueous media and pore solution leading to ingress of 319 sulfate ions into the pore structure of concrete. Two main potential gradients are 320 identified in the system. The chemical potential difference, named diffusion, results 321 in the transport of sulfate from high concentrated aqueous media to less 322 concentrated pore solution [115]. Electrical potential gradients result from the 323 variation of charge speeds in the solutions. In general, chemical, and electrical 324 potential gradients act together, creating a coupled electrochemical gradient. In 325 addition, difference in temperature can create a temperature gradient, and ionic flux 326 can also act as a transport mechanism [116, 117]. In nature, the transport of sulfate 327 ions to concrete's microstructure is a complex process involving all mentioned 328 mechanism, as well as some that were not considered.

329 ESA is often related to the damaging action of the products of chemical 330 reaction between sulfate ions and cement hydration products. The reactive 331 substances in concrete include pore solution and un-hydrated and hydrated solid 332 phases. Exact mechanism of chemical reaction in ESA depends on the nature, 333 concentration, and duration of sulfate exposure. Firstly, the influence of the nature 334 of the salt can be explained by the solubility and interaction mechanism of the

335 cations. Magnesium and sodium sulfate are the main sulfate salts associated with 336 ESA in concrete [118]. Magnesium sulfate has about 2 times higher solubility 337 compared to sodium sulfate. In addition, chemical reactions associated with 338 magnesium sulfate attack are considered more damaging due to its high reactivity. 339 Softening and disintegration of concrete matrix is due to low pH of the system 340 caused by transformation of CSH into MSH [119]. On the other hand, sodium 341 sulfate attack is associated with extensive formation of ettringite and gypsum which 342 generate

unbearable chemical and physical damage to the concrete matrix. The 343 most frequent chemical reactions are given in Eq. 2.3 to Eq. 2.5 [120-122].

344 $\square\square\square\square + \square\square\square\square_2\square\square\square\square_4 + 2\square\square \rightarrow \square\square\square\square\square\square\square + 2\square\square\square\square\square\square\square\square\square$ {2.3}

345 $\square\square_3\square\square + 3\square\square\square\square_2\square\square\square\square_4 + 3\square\square\square\square + 32\square\square \rightarrow \square\square_6\square\square\square\square_3\square\square_{32} +$

$6\square\square\square\square\square\square\square\square\square$ {2.4} 346 $3\square\square_4\square\square\square\square\square\square_{12} + 3\square\square\square\square_2\square\square\square\square_4 \rightarrow$

$2\square\square_6\square\square\square\square_3\square\square_{32} + 6\square\square\square\square\square\square\square\square\square + 2\square\square\square\square(\square\square\square\square)_3 + 21\square\square$ {2.5} 347

where, $C_6AS_3H_{32}$ is ettringite, the mineral responsible for expansion of concrete 348 under ESA, it has expansive factor between 0.5 to 1.5. Formation of gypsum is 349 related to certain concentrations and pH of the solutions. As an illustration, gypsum 350 is more likely to form from a precipitation in high concentration of sulfate ions 351 [123, 124]. This study focuses on the sodium sulfate attack in RPC. 352 Accumulation of expansive products in the concrete porous media results 353 from the continuous chemical reactions. The expansive forces generated by reaction 354 products cause the microcracking and internal damage of concrete microstructure. 355 Prolonged exposure to sulfate results in the prolonged chemical reaction 356 occurrence, which in turn, leads to formation and accumulation of more expansive 357 products [125]. There are two main theories describing the action of expansive 358 products on concrete matrix.

359 The first is volume increase theory. Accordingly, expansion of concrete 360 occurs due to additional volume generated from the expansive products of the ESA 361 chemical reaction [120, 121]. Expansive products of ESA chemical reaction usually 362 take more space than reactants. Volume increase theory considers volume change 363 of solid phases (both reactants and products). The volume of aqueous change is 364 considered unchanged. Linear expansion is expressed as a function of volume 365 change. Nevertheless, the exact correlation between volume of the ESA expansive

366 products and linear expansion is not documented [125]. More abundant approach is 367 crystallization pressure theory. Accordingly, the expansion is a results of 368 crystallization pressure which expansive products generate on the pore walls of 369 concrete [126, 127]. Eq. 2.6 can be used to express the pressure generated by the 370 ettringite with molar volume V_{Et}, ionic activity product Q_{Et} and equilibrium constant 371 K_{Et}.

$\square\square = ^{\square\square\square\square}$

$$\Delta G_{Et} = RT \ln\left(\frac{Q_{Et}}{K_{Et}}\right) \quad \{2.6\}$$

There are two main assumptions in the theory. Firstly, the solution is supersaturated, which means that ionic activity product Q_{Et} is greater than equilibrium constant K_{Et}. Secondly, ettringite crystals grow in confined pore space to exert the pressure on the pore walls [127, 128]. Hence, the expansive force generated depends on the location of ettringite crystal rather than total volume [126, 128-130]. Hence, considerable expansion of concrete does not necessarily result in the ESA related damage. In addition, pore spaces in concrete are generally empty, which gives them a potential for accommodation of expansive products. Hence, concrete pores can act as deposits for expansive ESA products [121, 131-133]. Number of studies reported the positive effect of high porosity of cementitious material under ESA [134-136]. Thus, the exact mechanism of sulfate attack and its quantification is still an ongoing topic of research.

Transport, chemical reactions, and expansive forces are the processes related to concrete's microstructure during the ESA damage. On the other hand, the mechanical response of concrete often occurs at macroscale. The term mechanical damage refers to micro and macrocracking of concrete as a results of generated damage products. Nevertheless, since the exact mechanism of ESA is still not understood fully, the cracks may occur in the region that are not directly exposed to sulfate because of complex compressive and tensile stresses generated in the concrete matrix [113].

Number of mixture design parameters influence the performance of cement-based materials subjected to ESA. One of the main factors controlling the durability of concrete is w/b. Relatively low w/b (less than 0.35) ensure high strength and low permeability of concrete [137]. However, this does not necessarily

result in improved ESA resistance. Number of research suggest that lowering w/b restricts the penetration of sulfate ions into concrete matrix, resulting in improved ESA resistance [111, 127, 139]. On the other hand, it was investigated that lowering w/b resulted in higher expansion rate of blended cement concretes [140, 141]. It was argued that lowering w/b increases the onset of expansion; however, after the expansion is initiated, concrete with lower w/b tend to experience more severe

damage in ESA [141]. In general, increasing w/b tends to increase the damage to 404 concrete exposed to ESA.

405 Another important factor influencing the ESA resistance of UHPC is 406 addition of supplementary cementitious materials (SCM) like silica fume or fly ash. 407 Number of research suggests that improved porosity and matrix densification that 408 is achieved by addition of SCM leads to high ESA resistance in UHPC [143-145]. 409 On the other hand, positive effect of increasing porosity of concrete to improve its 410 durability properties is being investigated [135-137].

411 The term physical sulfate attack was introduced briefly in this chapter. It 412 refers to ESA related damage that occurs due to crystallization and precipitation of 413 sulfate in concrete. As a result, expansion, cracking, flacking and disintegration of 414 concrete occurs which in turn leads to decomposition of strength producing CSH 415 weaking and damaging the microstructure of cement-based materials [7, 146]. The 416 nature of ESA in the concretes exposed to drying and wetting cycles is more 417 complex compared to fully submerged structures [147]. It is argued that during the 418 wet periods, sulfate ions can penetrate the concrete and initiate chemical sulfate 419 attack, while during dry periods rapid evaporation of water results in crystallization of SO_4^{2-}

420 in pore structure of concrete in the process of sodium sulfate crystallization 421 [148]. The coupled effect of chemical and physical sulfate attack leads to more 422 severe deterioration of concrete subject to drying and wetting cycles [149-151]. In 423 terms of physical sulfate attack, implementation of SCM like SF results in the 424 improved resistance to ESA under drying and wetting cycles [152-154]. In addition, 425 lowering w/b resulted in better performance of concrete with SCM both under 426 chemical and physical sulfate attack [155, 156]. Nevertheless, the effect of mixture

427 design parameters on the performance of UHPC exposed to ESA under wetting and 428 drying cycles is barely investigated.

429 Physical sulfate attack in concrete is also controlled by the exposure 430 conditions. Thus, it was investigated that duration of dry-wet cycles has a 431 considerable influence on the concrete performance under ESA [147, 157-159]. It 432 was investigated that variation of temperature has a considerable negative influence 433 on the ESA resistance

of cement-based materials exposed to dry-wet cycles [160]. 434 The main findings of the research related to dry-wet cycles ESA exposure of 435 concrete state that concrete experiences more severe deterioration when exposed to 436 sodium sulfate which is possibly due to higher rate of crystallization of Na_2SO_4 437 compared to $MgSO_4$. In addition, number of exposure factors including RH, 438 exposure duration, and duration of dry-wet cycles influence the macro and 439 microstructural changes in concrete exposed to ESA under dry-wet cycles [161]. 440 Hence, behavior of UHPC exposed to ESA under dry-wet cycling conditions 441 requires comprehensive research.

442 2.3.2 Freezing and thawing damage

443 Another important durability issue in UHPC, especially in regions affected by cold 444 environments is the effect of freezing-thawing (FT) cycles. As any other concrete, 445 the performance of RPC under FT cycles is governed by the properties of raw 446 materials, mixture design, curing and exposure conditions. FT damage in concrete 447 is induced by 9% of volume expansion of water upon freezing [162]. Expansion of 448 water in capillary pores of the paste matrix results in expansion and cracking. The 449 damage of FT cycles to concrete microstructure is the most frequently studied by 450 the accelerated laboratory testing. The most severe cases of FT damage led to 451 complete disintegration and surface spalling of concrete under repeated action of 452 FT cycles. The extend of FT induced damage in concrete is usually addressed by 453 pore refinement through reduction of w/b and/or addition of suitable admixtures 454 [42]. It was investigated that reduction of air voids size has more positive effect on 455 FT resistance of concrete compared to their spacing [163]. Adding SCM like fly 456 ash or SF can considerably reduce the air voids in concrete, hence, decreasing the

457 amount of water available for freezing. Nevertheless, implementation of air 458 entraining admixtures is limited in concrete with SCM due to the reduction of 459 capillary voids size [164]. In general, it was investigated that addition of SF and 460 decreasing w/b (as low as 0.35) had a positive effect on FT resistance of concrete 461 [145, 165, 166]. FT resistance of UHPC with different w/b was evaluated. It was 462 investigated that decreasing w/b in UHPC can significantly decrease the mass and 463 strength loss even at high number of FT cycles [167-170]. In addition, increasing 464

steel fiber content and application of special curing conditions were also proven to 465 have a positive influence on FT resistance of UHPC by number of studies [159, 466 171, 172]. Nevertheless, it is worth to mention that both increasing steel fiber 467 content and high temperature curing that were used in some studies to improve FT 468 resistance of UHPC can significantly increase the cost of UHPC production [23, 469 173, 174].

470 Number of studies attempted to evaluate the influence of FT cycles on 471 UHPC performance. However, most of the studies are restricted by the single factor 472 approach while the multiple factor impact is not fully investigated. In addition, the 473 significance of different mixture design in UHPC in its FT resistance is still ongoing 474 topic of research.

475 2.4 Modeling ESA

476 It is impossible to underestimate the importance of evaluating the performance of 477 concrete under the damaging action of ESA. Majority of research aimed to model 478 the ESA damage in concrete consider one or several of the fundamental ESA 479 mechanisms, namely, transport process, chemical reaction, expansive forces, and 480 mechanical response.

481 As it was introduced in previous sections, ionic transport between concrete 482 pore

space and aqueous salt containing media is caused by electrochemical potential gradient and advection [113]. Hence, enumerating ionic flux is the main term for ESA models that are based on transport process. The flux is computed as a function of diffusion, concentration, electrochemical potential, temperature, and velocity of liquid phase [116]. Nevertheless, transport mechanism-based models are often limited by the assumption of volumetric water content being equal to the total porosity of the concrete [175]. In addition, relatively high number of factors of consideration make simulation by these models take considerable computational effort, resulting in the reduction of factors of consideration which, in turn, limits the model precision [116, 176, 177]. More simplified approach is to quantify diffusivity through strength loss, cracking, and spalling. In other words, increase in diffusivity is modeled by bulk damage or generated crack dimension [122, 133, 178-183].

Modeling ESA in concrete through chemical reactions has two distinct approaches. Firstly, it is modeling through kinetic laws. In this method partial differential equations are used to compute the consumption of reactants or precipitation of products via empirical reaction rate constant. Thus, sulfate and/or aluminate consumption and ettringite precipitation are considered in these models [179, 182, 183-186]. Gypsum formation was considered only in limited number of models [181, 187]. The general rate law of chemical reactions considered when modeling ESA in concrete is provided in Eq. 2.7 and 2.8.

$$\frac{d[SO_4^{2-}]}{dt} = -k_1[SO_4^{2-}] \quad \{2.7\}$$

$$\frac{d[SO_4^{2-}]}{dt} = -k_2[SO_4^{2-}][Ca^{2+}] \quad \{2.8\}$$

where, k_1 and k_2 are first and second order reaction rate constants. Different terms are used to express the units of reaction rate constant which is $time^{-1}$. Using first order reaction law is limited by the assumption that no change in concentration of portlandite occurs throughout the ESA which can be overcome to certain extent by restricting the formation of ettringite through initial sulfate concentration [187]. Nevertheless, the most common approach is to use second or multi-ordered reaction rate [181, 188]. The effect of concentration and solution temperature can be modeled by using second order rate law and Arrhenius equation.

It is assumed that 513 chemical reaction occurs in two distinct steps with different reaction rates [189- 514 191]. The approach allows to simplify the modeling through evaluation the 515 expansion of concrete. Another purely empirical approach to modeling ESA is 516 through the laws of chemical equilibrium. Chemical equilibrium requires all phases 517 of the system to be in the state of minimal Gibb's energy. Law of mass action which 518 is used to solve the equation of mass balance in the system of concrete and sulfate 519 [192]. Mass and charge balance aimed to minimizing Gibb's free energy is another 520 approach to model the chemical reactions in ESA in concrete [116, 178, 180, 193- 521 196]. However, number of studies also showed the complexity of integration 522 chemical equilibrium into coupled chemo-transport models [175, 178, 180, 193, 523 197]. Hence, some studies suggested to use combination of kinetic laws and 524 chemical equilibrium to express the chemical processes of ESA in concrete [178, 525 180, 187, 193]. The kinetic laws are used to describe the ettringite precipitation, 526 and it is considered through equilibrium solubility product in the chemical 527 equilibrium of the system [187]. Nevertheless, models considering both kinetics 528 and equilibrium require considerable computational effort.

529 Volume increase theory models account for the "buffer" capacity of 530 concrete pores that can accommodate certain amount of formed expansive products. 531 Hence, generated pressures consider accumulated volumes or large size particles 532 only. Local linear expansion is expressed as the function of "buffered" volume of 533 expansive products and initial concrete porosity [113, 179]. The pore size 534 distribution of concrete requires more precise discretization to account for the 535 formation and accumulation rate of ettringite [133]. However, some studies totally

536 neglect the buffering capacity of pore network in concrete ESA modeling [186, 537 197]. There is a limited number of models that employ crystallization pressure 538 theory to quantify the expansive forces since it is not a commonly accepted method 539 in ESA mechanism theory and modeling. Only chemical kinetics without 540 equilibrium was used to express the chemical processes in such model [187, 198]. 541 The precision of the resulting model was found within acceptable range; however, 542 it resulted in the considerable underestimation of generated expansion. The problem 543 was minimized by application of volume increase theory.

544 The mechanical response of concrete exposed to ESA was addressed in 545 almost every existing model. The common approach was to assume linear stress 546 strain relationship, which allow to consider local one-dimensional strains as 547 representatives of the stress that is endured by the system [122, 177, 179, 183]. The 548 major associated simplifications include the following: the material initially is 549 within linear-elastic response range followed by microcracking and steady decrease 550 of mechanical properties which leads to accumulation of microcracks and formation 551 of macrocracks which significantly decreases the load carrying capacity of the 552 matrix. Explicit cracking, and the influence of crack propagation can be addresses 553 by the models based on this assumption [122, 184, 187]. Nevertheless, only limited 554 number of models consider chemically induced damage through a local relative 555 strength loss [181, 186, 199]. The most recent additions to modeling the mechanical 556 response is made by considering the effect of the size and shape of the specimen on 557 the ESA resistance of cement-based material structure [131, 200]. Hence, number 558 of models exists that consider one or more aspects of ESA in concrete, and the most 559 important step is to choose the model that will suit the aims and objectives of the 560 research.

561 Even though some assumptions made to apply the model might lead to its 562 simplification, complexity of the model does not necessarily represent its precision 563 in expressing and/or evaluation the ESA in concrete. On the other hand, model 564 complexity leads to considerable increase of computational effort, which limits the 565 application. In addition, it is worth to mention that reviewed models were applied

566 only for OPC or blended concretes, while modeling ESA resistance of RPC is a 567 topic of current study.

568 2.5 Modeling FT

569 One of the main contributions of current research is to evaluate the RPC's durability 570 under FT damage both experimentally and through simple yet comprehensive 571 model. FT cycles induced damage can result in the failure of structures especially 572 in cold climates [201]. In general, FT induced damage in concrete is associated with 573 two aspects: firstly, freezing and volume increase of capillary water resulting in 574 micro and macrocracking, and secondly, frost action on surface water which leads 575 to surface scaling [202]. In both cases degree of saturation of concrete which is the 576 quantification of the amount of the moisture inside and outside the concrete plays a 577 crucial role. It is worth to mention that water present in gel pores of concrete can 578 freeze if temperature falls bellow -75 ºC which is not always achievable even in 579 laboratory conditions [203]. In addition, pressures generated by 9% volume 580 increase of water can be accommodated by pore space of concrete without cracking 581 or other internal damage [204]. Another important factor of consideration is 582 hydraulic pressure which is governed by Darcy's law where pressure gradient is a 583 function of viscosity, concrete permeability, flow area and rate, and the length of 584 flow path. Hydraulic pressure is generated as a resisting force to flow of unfrozen 585 water in the matrix [205]. Hence, the pore structure of concrete can be improved by 586 increasing air voids spacing through mixture design. In addition, it is necessary to 587 consider the osmotic pressure generated by water and solvent in gel pores of 588 concrete [205]. It might be suggested that pore size is the main governing factor in 589 FT resistance of concrete; however, number of studies emphasized the importance 590 of pore spacing, connectivity and distribution in effective FT durability of cement 591 based materials [167, 206-209]. As it was mentioned previously, addition of SCM 592 including SF make RPC potentially high resistance to FT action.

593 Evaluation of FT resistance of concrete is conveniently performed through 594 durability factor (DF) and relative dynamic modulus of elasticity (RDME). 595 Nevertheless, the classical method of RDME and DF calculation often lead to 596 overestimation of concrete's FT resistance [210, 211]. On the other hand, 597 modifying DF through including relevant terms like the porosity, permeability or 598 strength of concrete can improve its ability to express the FT resistance of cement-

599 based materials [212, 213]. Notwithstanding the numerous attempts to model the 600 FT damage empirically associated assumption often resulted in either 601 oversimplification of model or in the increased computational effort. Thus, 602 Boltzmann equation was used to express the relationship between the mass loss 603 rate, cumulative damage, and number of FT cycles in aerated concrete [214]. 604 Another approach was to simulate the ITZ, aggregates and air voids distribution in 605 concrete subjected to FT damage through trans-scale finite element model [215]. 606 However, the model was limited by the overestimate of pore saturation in concrete. 607 In addition, transferring model from two-dimensional to three-dimensional scale 608 resulted in the considerable decrease of accuracy and increase of computational 609 effort. Hence, this research is focused on application of simple but sophisticated 610 modeling of FT damage based on DF that was previously used for OPC and blended 611 concretes to RPC since evaluation of FT performance of UHPC is newly emerging 612 research topic and requires efficient investigation and development.

1 3. Materials and Methods

2 Verification of RPC properties, as well as development of its resistance models was based 3 on number of experimental tests which included both conventional concrete testing 4 methods and novice experimental and statistical tools. This chapter describes all testing 5 methods, raw materials, design of experiments and experimental setup used for the 6 dissertational research.

7 3.1 Materials and Sample Preparation

8 This section describes characteristics of the raw materials, and standardized mixing 9 procedure used for RPC mixing. RPC is a special type of concrete that consists of cement 10 and SF as binder materials, fine quartz river sand as fine aggregate and ordinary tap water. 11 Additional materials can be used to improve the properties of RPC. Liquid 12 superplasticizer (SP) is used to increase workability of low w/b mixtures. Steel or mineral 13 fibers can be employed to enhance strength and ductility characteristics or RPC. In the 14 current study steel fibers were used in some mixtures.

15 3.1.1 Binders

16 Locally available ASTM Type I ordinary Portland cement and densified SF were 17 used as binder materials for RPC in this study for the whole sets of experiment. Properties 18 of binders are given in Table 3.1.

19 Table 3.1. Properties of binders.

Component	Cement	SF
Chemical composition (% mass)		
CaO	62.73	0.22
SiO2	20.78	97.5
Al2O3	4.82	0.2
Fe2O3	3.95	0.5
SO3	3.14	0.12
MgO	1.57	0.56
Na2O	0.78	0.25
K2O	-	0.56
Minerology		
C3S	64	-

Table 3.1. Properties of binders (cont.)

Component	Cement	SF
C2S	15	-
C3A	6	-
C4AF	12	-
Physical properties		
Specific surface area (m2/kg)	421	2300
Specific gravity	3.15	2.22
Loss on ignition	2.08	2.08

Ordinary tap water was used for RPC mixing in proportions required by mixture design.

3.1.2 Aggregate

Fine quartz sand with properties as given in Table 3.2 was used as fine aggregate for RPC mixtures.

Table 3.2. Properties of fine aggregate.

Property	Bulk specific gravity		Fineness modules		Characteristic diameter
			Absorption capacity		
Units	[%]	[mm]	Value	2.4	1.02	6.2	0.97	Gradation
Sieve size	[mm]	4.75	2.36	1.18	0.6	0.3	0.15	0.075	Pan	Retained on sieve [%]	0	0	0	2.3	29.8	53.9	13.5	0.4	0	Total passing	100	100	100	97.7	67.9	14	0.4	0

Properties of locally available quartz sand were modified by Toufar model to improve the packing degree, and RPC properties. The details are discussed in the following chapters.

3.1.3 Supplements

Steel fibers with Ø 0.16 mm and 13 mm length were used in this study in the parts of experiments where properties of RPC with steel fibers were investigated. Liquid superplasticizer (SP) Master Glenium ACE 430 with specific gravity 1.02 was added to RPC mixture at different dosage to ensure suitable workability of the mixtures.

Locally produced sodium sulfate with 98% purity was used for making ESA exposure solutions. Sodium sulfate has a molecular formula of Na_2SO_4 and referred as

sodium sulphate in number of written works. These three terms will be used

interchangeably throughout the body of the thesis. There are many ways to express the concentration of solution. Table 3.3 provides a guidance for calculating and transferring the concentrations of sodium sulfate from one unit to another.

Table 3.3. Sodium sulfate solution concentration guide.

Molar masses

Molar mass of Na_2SO_4 23×2+32+16×4 = 142 g/mol

Molar mass of SO_4^{2-} 32+16×4 = 96 g/mol

Typical concentrations of Na_2SO_4

Molar concentration 1M, or 1 mol/L 1×142 = 142 g/L Mass concentration 1%, or 1 g/100 g 1×1000÷100 = 10 g/L Typical concentrations of SO_4^{2-}

Particles per million, ppm 1 ppm, or 1 mg/L 1÷1000 = 0.001 g/L Examples

0.35M Na_2SO_4 = 0.35 mol/L × 142 g/mol = 49.7 g/L.

5% Na_2SO_4 = 5 × 1000/100 = 50 g/L.

50 g/L Na_2SO_4 = 50 g/L ÷ 142 g/mol = 0.35 mol/L = 0.35M.

10,000 ppm SO_4^{2-} = 10,000 mg/L = 10 g/L = 10 g/L ÷ 96 g/mol = 0.10 mol/L = 0.1M.

0.35M Na_2SO_4 = 0.35M SO_4^{2-} = 0.35 mol/L = 0.35 mol/L × 96 g/mol = 33.6 g/L = 33,600 mg/L = 33,600 ppm.

The salt was dissolved in deionized water to produce sulfate solutions of specified molar concentrations. Solutions were renewed every 3 months for all sets of experiments to ensure continuous exposure to stable concentrations of salt.

3.1.4 Mixing procedure and sample preparation

Mixing of RPC was carried out following the procedure described in Fig. 3.1 mixing was carried out in either 100 L capacity pan-type mixer for mixing large volumes of RPC, or in 2 L capacity mortar mixer for preparation of small volume of RPC specimen. Mix time is 9±1 min.

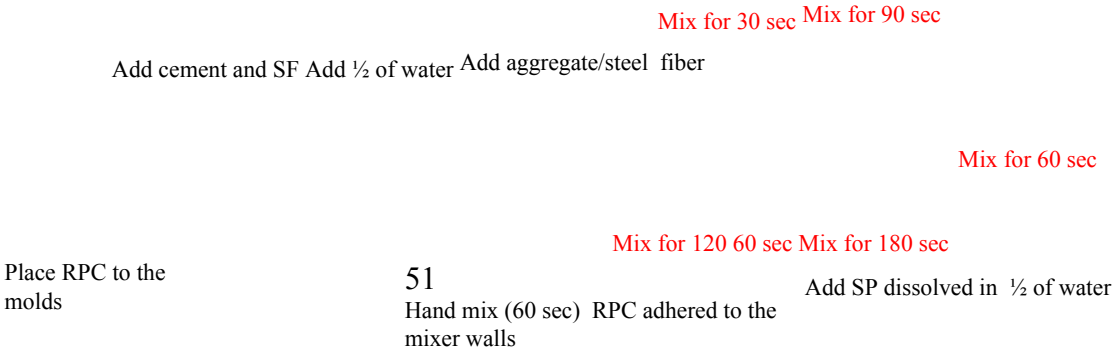

Fig. 3.1. Mixing procedure for RPC.

Specimen were cast in two or three layers based on the size and shape of the molds. Rubber or metal stick was used to tap each layer. Improved compaction was achieved by shaking the molds. Excess concrete was removed from the top layer with the help of metal scraper. Plastic sheets were used to cover the specimen to avoid evaporation. Specimen were cured in molds for 24 hours, and demolded. Further operations depended on the aim and methods of the testing that are described in the next chapter.

3.2 Testing program

Number of tests were performed on raw material, fresh and hardened, unexposed and damaged RPC samples to analyze its quality, strength, and durability properties. Standardized testing methods developed for ordinary Portland cement concrete and hydraulic mortars were employed for RPC. The precision, accuracy and statistical variance

of the results were ensured by using more than 3 samples, and/or by making 65 more than 3 readings/observations per experiment for each RPC mixture. In addition, 66 ASTM Standard E178 principle was used to eliminate outlying observation from the tests 67 that contained more than 4 samples/readings [216].

68 3.2.1 Aggregate properties

69 Several tests were performed to determine the qualities of raw sand, and to modify its 70 characteristics.

71 *Sieve analysis of fine aggregate*

72 Particle size distribution of fine aggregate is determined by the test method following the 73 procedure described in ASTM C136 [217]. The procedure for testing is as following:

1) The sample is dried to a constant mass at 110±5 ^{0} 74 C. 75 2) The sieves with suitable openings (1.18 mm, 600 µm, 300 µm, 150 µm, 76 75 µm as specified by [218] were chosen for testing.

77 3) The sieves were nested on testing apparatus, and agitated automatically 78 for 10 min.

79 4) Mass of samples retained on each sieve was measured.

80 Total mass of the material after sieving was kept close to original mass of the sand. 81 Individual percent retained is the percentage of material retained on a sieve with certain 82 size. Cumulative percent retained is calculated as successive sum of individual percent 83 retained for each subsequent sieve. Fineness modulus of the sand is calculated as total 84 percent retained by sieves 1.18 mm, 600 µm, 300 µm and 150 µm divided by 100.

85 *Relative density and absorption of fine aggregate*

86 Standard fine aggregate testing method as specified by ASTM C128 [219] was performed 87 to identify the relative density (specific gravity) and absorption of fine aggregates. Raw 88 material was prepared for the test by following the procedure as described:

1) Sand was oven dried at 110±5 ^{0} 89 C to a constant mass. 90 2) Sand was covered with water for 24±4 h.

91 3) The excess water was decanted to avoid the loss of fines. 92 4) Sand was spread on a flat non-absorbent surface.

93 5) Tumbling and stirring were used to ensure free flow of air into the sand 94 sample.

95 6) The specimen was air dried until saturated surface dry condition is 96 reached.

97 Fig. 3.2 provides schematic representation of different moisture conditions of fine 98 aggregate to illustrate the aggregate testing method presented.

Wet Saturated surface dry
Air dry Oven dry

99

100 Fig. 3.2. Moisture conditions of fine aggregate.

101 The procedure for gravimetric testing is as following:

102 1) The pycnometer was partially filled with water.

103 2) 500±10 g of saturated surface dry fine aggregate was introduced into the 104 pycnometer.

105 3) The pycnometer was filled with additional water to 90 % of capacity. 106 4) The pycnometer was manually rolled and inverted to eliminate any visible 107 air bubbles.

5) Constant 23±2 ^{0}
108 C temperature was ensured.

109 6) The pycnometer was filled with water up to 100 % level. 110 7) The pycnometer with sand sample and water was weighed.

111 8) Fine aggregate was removed from pycnometer, and oven dried at 110±5 ^{0}
112 C to a constant mass.

113 9) The mass of sample was determined after cooling at room temperature for 114 1±½ h.

115 10) The mass of pycnometer filled with water to 100 % was determined.

116 The characteristics of fine aggregate were determined based on Eq. 3.1 to 3.4. 117

[illegible] [illegible] ([illegible] [illegible])([illegible]) = [illegible]/([illegible] + [illegible] − [illegible]) {3.1} 118
[illegible] [illegible] ([illegible] [illegible])([illegible]) = [illegible]/([illegible] + [illegible] − [illegible]) {3.2} 119
[illegible] [illegible] [illegible] ([illegible] [illegible]) = [illegible]/([illegible] + [illegible] − [illegible]) {3.3} 120 [illegible], % = ([illegible] − [illegible])/[illegible] × 100 {3.4}

121 where, *A* – oven dry mass, *g*, *B* – mass of pycnometer, filled with water to 100 %, 122 *g*, *C* – mass of pycnometer, filled with water and sand to 100 %, *g*, *S* – saturated surface 123 dry mass, *g*.

124 *Moisture content of fine aggregate*

125 Moisture content of fine aggregate was determined as specified by ASTM C566 test 126 method [220]. The procedure for determination of moisture content is to measure the mass 127 of the sand sample representative of its normal conditions, oven dry the sample at 110±5 ^{0} 128 C to a constant mass and measuring the oven dry mass. Moisture content of the fine 129 aggregate is calculated as in Eq. 3.5.

$$[illegible] = \frac{[illegible]-[illegible]}{[illegible]} \times 100 \quad \{3.5\}$$

130

$$[illegible]$$

131 where, *MC* – moisture content, *%*, *MC* – moisture content, *%*, *W* – mass of sand 132 specimen, *g*, W_{OD} – mass of oven dried sand specimen, *g*.

133 *Bulk density and voids of fine aggregate*

134 Bulk density (unit weight) of aggregate and percentage of voids between particles is 135 determined as specified in ASTM C29 [221]. The procedure for determination of unit 136 weight and voids is as following:

1) The sample of sand was oven dried at 110±5 ^{0} 137 C to a constant mass. 138 2) Container of a known volume was filled with 3 equal and subsequent 139 portions of sand.

140 3) Each layer was rodded and tamped 25 times.

141 4) The mass of the container was measured.

142 The bulk density (dry rodded unit weight) and air voids in aggregate were calculated 143 as specified by Eq. 3.6 and Eq. 3.7.

144 $$M = (G - T)/V$$ {3.6}

$$\% \text{ Air voids} = \frac{(S \times W) - M}{S \times W}$$

145 {3.7}

where, M – dry rodded unit weight (bulk density), g/cm^3

146 , G – mass of aggregate and container, g, T – mass container, g, V – volume of the container, cm^3

147 , S – bulk specific gravity determined by Eq. 3.2.1, W – density of water, g/cm^3

148 .

149 3.2.2 RPC fresh properties

150 Several tests were performed to investigate the fresh properties of RPC. Fresh properties 151 of concrete allow to assess the quality of the mixture as well as to provide information on 152 the hydration process of RPC. These tests were performed immediately after mixing of 153 RPC was complete.

154 *Flow table test*

155 Standard flow test as specified in ASTM C1437 [222] was performed to check the 156 workability of RPC. The test method is designed specifically to test the workability of 157 hydraulic cement mortar. The procedure for determination of flow is as following:

158 1) Flow table was wiped dry and clean.

159 2) The flow mold was placed at the center of the flow table. 160 3) A layer of mortar about 25 mm thick was placed in the flow mold and 161 tamped 20 times with the tamper.

162 4) The mold was filled with second layer of the mortar and tamped as 163 specified by for the first layer.

164 5) Excess mortar was cut off to a plane surface by a straight edge tool with a 165 sawing motion.

166 6) The tabletop was wiped dry and clean to remove any mortar or liquid drops 167 on the surface.

168 7) The mold was lifted away from the table.

169 8) The table was dropped immediately 25 times in 15 sec.

170 9) The diameter of the mortar along the 4 lines scribed in the tabletop was 171 measured by caliper to the nearest millimeter,

172 The flow area is calculated as given in Eq. 3.8. The average of 4 readings is 173 reported.

$$\Gamma_{\diamond\diamond} = \frac{(\diamond\diamond_1 \times \diamond\diamond_2) - \diamond\diamond_0^2}{\diamond\diamond_0} \quad \{3.8\}$$

174

175 where, Γ_m – relative flow area; d_1 and d_2 – diameter of the mortar circle, *mm*; d_0 – 176 diameter of the original inside base, *100 mm*.

177 The workability of RPC can be reported as a flow diameter as given in Eq. 3.9. 178

$$\diamond\diamond_{\diamond\diamond} = \diamond\diamond - \diamond\diamond_0 \quad \{3.9\}$$

179 where, d_f – flow diameter, *cm*; d – the average of 4 diameter readings, *cm*; d_0 – 180 diameter of the original inside base, *10 cm*.

181 *Setting time*

182 The setting time of RPC mixtures was determined according to ASTM C403 [223]. The 183 testing apparatus consists of penetration needles of different size (645, 323, 161, 65, 32 and 16 mm^2

184) installed 25 mm away from the mortar area and spring-reaction type loading 185 apparatus with maximum 600 N penetration force, and accuracy of ±10 N. The setting 186 time of RPC was measured in standard room temperature and humidity. The testing and 187 calculation procedure based on the standard test method is as following:

188 1) The needle of appropriate size (depending on the degree of concrete 189 setting) was inserted into the mortar.

190 2) Gradual and uniform force was applied by the apparatus from the moment 191 when needle contacted the surface of the specimen till the 25 mm penetration depth 192 (approximate time is 10±2 sec.

193 3) The time of application (time elapsed form the moment of initial contact 194 of water to cement) and force required to produce the penetration were reported. 195 4) At least six penetrations were performed for each mixture, with time 196 intervals that ensure satisfactory curve. Penetration resistance should be equal to or exceed 27.6 N/mm^2

197 .

Penetration resistance of mixtures (N/mm^2
198) was plotted versus time elapsed (min) 199 on log-log scale. The times of setting were determined from the plot by linear regression

200 analysis of the logarithms of the data. The data was fitted into Eq. 3.10 to determine 201 regression constants.

202 ������(����) = ?? + ?????????(??) {3.10}

where *PR* – penetration resistance, N/mm^2
203 ; *t* – elapsed time, *min*; *a* and *b* – 204 regression constants. The times of initial and final setting were determined from Eq. 205 3.2.10 as times corresponding to 3.45 and 27.58 MPa respectively.

206 3.2.3 RPC hardened properties

207 Hardened properties of RPC were determined to be understand the characteristics of the 208 material and to assess its properties both while undamaged and after exposures to ESA 209 and FT cycles.

210 *Density, Absorption, and Voids*

211 Ø 100 mm and 200 mm length cylindrical specimen were used for determination of 212 density, absorption and air voids in RPC as specified by ASTM C642 [224]. Mass of RPC 213 specimen at 4 different conditions was reported.

214 1) Oven-dry Mass, *A* – the mass of RPC specimen after drying in the oven at 100 to 110 ^{0}
215 C temperature for at least 24 hours.

216 2) Saturated Mass After Immersion, *B* – the mass of RPC specimen after 217 immersion in water at room temperature for at least 48 hours.

218 3) Saturated Mass After Boiling, *C* – the mass of RPC specimen after boiling 219 in water for 5 h. Sample were naturally cooled for not less than 14 h. 220 4) Immersed Apparent Mass, *D* – the mass of RPC specimen suspended in 221 the water by a wire.

222 The calculations were performed as specified by Eq. 3.11 to Eq. 3.17.

?????????????????????? ??????????

[illegible], % = [[illegible]−[illegible]
223] × 100 {3.11} [illegible]
[illegible] [illegible]
[illegible] [illegible] [illegible], % = [[illegible]−[illegible]
224] × 100 {3.12} [illegible]
[illegible] [illegible], [illegible], [illegible]1 = [[illegible]
225] × [illegible] {3.13}
[illegible]−[illegible]
[illegible] [illegible] [illegible]
[illegible] = [[illegible]
226] × [illegible] {3.14} [illegible]−[illegible]
[illegible] [illegible] [illegible]
[illegible] [illegible] [illegible] = [[illegible]
227] × [illegible] {3.15}[illegible]−[illegible]

[illegible] [illegible], [illegible]2 = [[illegible]
228] × [illegible] {3.16}
[illegible]−[illegible]
[illegible] [illegible] [illegible]
[illegible] [illegible] ([illegible]), % = [illegible]1−[illegible]2
[illegible]2× 100 = [illegible]−[illegible]
229 × [illegible]−[illegible]
230 100{3.17}
231 where ρ – density of water.
232 *Sorptivity*
233 The rate of absorption of water, or sorptivity, of RPC was measured in accordance with 234 ASTM C1585 [225] testing procedure. Ø 100 mm and 50 mm length cylindrical specimen 235 water cured for 14 days in room temperature lime saturated water. As a part of preparation
to the experiment specimen were put in the environmental chamber at 50±2 ^{0}236 C 237 temperature and 80% relative humidity for 3 days. Afterwards, specimens were put in a 238 sealable container to be stored at room temperature for 15 days. As the final step of 239 preparation to the testing the side surface of specimen were sealed with the tape. The 240 diameter of unsealed part side was measured 4 times and recorded. The testing procedure 241 was as following:

242 1) The mass of specimens were measured to the nearest 0.01 g. 243 2) The support device

was placed at the bottom of the pan. 244 3) Pan was filled with tap water so that the water level is 1 to 3 mm above 245 the top of support device.

246 4) The timing was started at the moment when the specimen was placed on 247 the support device on its unsealed side.

248 5) The mass of the specimen was measured at the following time intervals: 249 60 s, 5 min, 10 min, 20 min, 30 min, 60 min, every hour up to 6 h, once a day up to 7 250 days, and one measurement between day 7 and 9.

251 The absorption is calculated as specified by Eq. 3.18.

$$I = \frac{m_t}{a \times d} \quad \{3.18\}$$

252

253 where, I – the absorption, mm; m_t – the change in specimen mass at time t, g; a – the exposed area of the specimen, mm^2; d – density of water, g/mm^3

254 . The initial rate of water absorption, also referred as initial sorptivity ($mm/s^{1/2}$ 255), is 256 determined as the slop of the best fit line for I plotted versus $\sqrt{t}$ for using the data from 1 257 min to 6 h measurement. The secondary rate of water absorption, also referred as initial

sorptivity ($mm/s^{1/2}$ 258), is determined as the slop of the best fit line for I plotted versus $\sqrt{t}$ for 259 using the data from 1 day min to 7-day measurement.

260 *Drying Shrinkage*

261 The drying shrinkage of RPC was determined in accordance with the procedures 262 described in ASTM C157 and ASTM C490 testing standards [226, 227]. Linear variation 263 of beam samples with 25×25 mm cross section and 250 mm length along longitudinal 264 axis were measured with a digital length comparator with ±0.0001 mm accuracy is used 265 for the measurement. The specimens were stored in an environmental chamber with the temperature $23\pm2\ ^0$

266 C, and 50 % RH. The drying shrinkage value was calculated using Eq. 267 3.19.

$$L = \frac{L_x - L_i}{G} \times 100 \quad \{3.19\}$$

268

269 where, L – length change, *%*; L_x – (comparator reading of specimen at x age) - 270 (comparator reading of reference bar at x age), mm; L_i – (initial comparator reading of 271 specimen) - (initial comparator reading of reference bar), mm; G – nominal gauge length, 272

250 mm.

273 *Ultrasonic Pulse Velocity*

274 The propagation velocity of longitudinal stress wave pulses through RPC is measured 275 following the guidelines of ASTM C597 test method [228]. The pulse velocity is related 276 to concrete's elastic properties as given in Eq. 3.20.

$$\text{[illegible]} = \sqrt{\frac{\text{[illegible]}(1-\text{[illegible]})}{\text{[illegible]}(1+\text{[illegible]})(1-2\text{[illegible]})}}$$

277 {3.20}

278 where, V – pulse velocity through concrete, *m/s*; E – dynamic modulus of elasticity, *MPa*; μ - dynamic Poisson's ratio; ρ – density, kg/m^3

279 .

280 The test is used to evaluate the uniformity and relative quality of concrete. 281 Homogeneous concretes without structural microcracks tend to have velocity about 4000 282 m/s. The procedure for measuring longitudinal pulse velocity through RPC is as 283 following:

284 1) Verification of the correct operation of equipment is made before 285 measuring each new mixture of RPC.

286 2) An appropriate amount of coupling agent is a applied to the face of 287 transducers.

288 3) The transducers are placed firmly against the surface of the RPC sample.

289 Average of 9 reading per sample is reported as ultrasonic pulse velocity. 4 samples 290 are measured for each RPC mixture.

291 *Dielectric conductivity*

292 Dielectric conductivity of concrete is its resistance to the movement of ions under applied 293 electric field. In other words, it indicates how readily ions can be transported through the 294 concrete specimen via its gel pores and pore solutions. It can indicate the resistance of 295 concrete to penetration of harmful solutions, as chloride or sulfate. The correct working 296 conditions of apparatus were verified by applying the current to standard surface. The 297 dielectric conductivity of RPC is measured using 70 mm cube specimen. The average of 298 5 readings from five sides of the cubes were reported for each RPC mixture.

299 3.2.4 RPC strength tests

300 RPC strength test included compressive strength and modulus of rupture test both on 301 undamaged specimen, and on specimen exposed to ESA or FT damage. 302 *Compressive strength test*

303 Cube compressive strength of RPC was determined by test method specified by ASTM 304 C109 [229]. Cube compressive strength of RPC is used most frequently in this study; 305 hence, it will be referred as compressive strength of RPC. Accordingly, 50×50×50 mm 306 cubes that were compacted by tamping in two layers were broken on universal concrete 307 testing machine. The maximum load was recorded to the nearest 0.001 kN. The average 308 of 3 to 4 samples was reported.

309 Cylindrical compressive strength of RPC was determined as specified by ASTM 310 C39 [230]. Ø 100 mm and 200 mm length cylindrical specimen were broken on universal 311 testing machine. The maximum load was recorded to the nearest 0.001 kN. The average 312 of 3 to 4 samples was reported. Samples were tested in 2 different machines for 313 comparison purpose.

314 *Modulus of Rupture test*

315 RPC beam specimen were tested in accordance with testing method specified by ASTM 316 C293 [231]. 40×40 mm cross sectional beams with 160 mm length were used for 317 unexposed and ESA exposed RPC testing. 76.2×76.2 mm cross sectional beams with 287

318 mm length were used for FT damaged RPC testing. The average of 3 to 4 samples was 319 reported for each test. The modulus of rupture of RPC specimen was calculated as 320 specified by Eq. 3.21.

$$R = \frac{3PL}{2bd^2} \quad \{3.21\}$$

321

322 where, R – modulus of rupture, *MPa*; P – maximum applied load indicated by the 323 testing machine, *N*; L – span length, *mm*; b – average width of specimen, *mm*; d – average 324 depth of specimen, *mm.*

325 3.2.5 RPC durability tests

326 RPC properties were evaluated with standard test methods described in previous chapters

327 as well as with specific test to determine the durability properties of the material. 328 *ESA resistance of RPC*

329 ESA resistance of RPC was determined by length and mass change of RPC were 330 tested as in accordance with the ASTM C1012 [232]. 25×25 mm cross sectional beams 331 with 250 mm length were used for this test. The mass of the sample and its relative length 332 were measured with the help of high precision scales and special apparatus as specified 333 by ASTM C490 respectively [227]. Eq. 3.2.19 is used to calculate the length change, 334 while mass change is calculated as given by Eq. 3.22. the average of 3 to 6 samples were 335 used to report the final value for each tested RPC mixture.

$$\Delta m = \frac{m_x - m_i}{m_i} \times 100 \quad \{3.22\}$$

336

337 where, Δm – mass change, *%*; m_x – mass of specimen at *x* age, *g*; m_i – initial mass 338 of specimen, *g*.

339 The mass change of RPC specimen were measured as in accordance with the 340 following procedure: firstly, samples were taken out of the solution (water, in case of 341 freezing and thawing resistance test), then they were let dry in air for approximately 1 h; 342 lastly, prior to being put on the scales excess moisture (if any) was wiped with the dry 343 towel

344 *FT resistance of RPC*

345 FT resistance of RPC was evaluated based on the ASTM C666 Procedure A (rapid 346 freezing and thawing in water) testing method [233]. 76.2×76.2 mm cross sectional beams 347 with 287 mm length were used for testing. One cycle of FT testing consisted of freezing

to -18 ^{0}C and thawing to +18 ^{0}

348 C. The average duration of 1 cycle was about 6 hours. 349 Properties of RPC were measured after each 16 cycles, total 300 cycles were performed. 350 Mass and length of the specimen were measured with the use of high precision 351 scales and caliper as given by Eq. 3.22 and 3.23 respectively.

$$\Delta L = \frac{L_x - L_i}{L_i} \times 100 \quad \{3.23\}$$

352

353 where, ΔL – length change, *%*; L_x – length of specimen after *n* cycles, *mm*; L_i – 354 initial

length of specimen, *mm*.

355 Ultrasonic pulse velocity of beam samples was measured as in accordance with 356 ASTM C597 [228]. Relative dynamic modulus of elasticity (RDME) of RPC was 357 determined as given in Eq. 3.24.

$$P_c = \left(\frac{n_1^2}{n^2}\right) \times 100 \quad \{3.24\}$$

358

359 where, P_c – RDME after *n* cycles, n_1 – UPV after *n* cycles, *m/s,* n – UPV before FT 360 cycles, *m/s*.

361 Standard durability factor is determined as given in Eq. 3.25. 362

$$DF = P/N \quad \{3.25\}$$

363 where, *DF* – durability factor of the test specimen, *P* – RDME after *n* cycles, *N* – 364 number of cycles, *M* – specified number of cycles at which exposure is terminated (300).

365 3.2.6 RPC microstructural properties

366 Microstructural properties of RPC mixtures were examined using available technologies 367 including SEM observations along with Energy Dispersive X-Ray Spectroscopy (EDS), 368 mineralogical analysis by X-Ray Diffraction (XRD), and porosity measurement. 369 *SEM observations*

370 SEM observations were made using two apparatus. The first is SEM Crossbeam 540 by 371 Zeiss which scans the sample with a focused electron beam and delivers information on 372 topography and composition of the sample. The second is JSM-IT200 (LA) by Jeol. It is 373 user-friendly compact SEM that allows to obtain quality images and EDS analysis quickly 374 and efficiently. Samples for both apparatuses were prepared by application of 10 nm Au 375 coating. RPC samples subject to ESA were analyzed to assess microstructural changes 376 occurred.

377 *XRD analysis*

378 Mineralogical composition of RPC samples was analyzed by XRD analysis using XRD 379 system SmartLab by Rigaku. Apparatus has sophisticated features and employs 380 intelligent software. RPC samples subject to ESA were analyzed to evaluate the changes 381 in mineralogical composition.

382 *Porosity measurement*

383 Porosity of RPC samples was measured by Mercury Intrusion Porosimeter (MIP) 384 Poremaster 60 from Quantachrome Instruments. MIP measurement techniques is based 385 on non-wetting, non-reactive liquid penetrating fine pores under applied pressure. Pores 386 between 3.6 nm and 1100 μm can be measured.

387 3.3 Design of experiments

388 The main aim of this research is to develop RPC mixture with superior strength and 389 durability properties from locally available material as well as to establish the 390 mathematical

model between input variables and output signal. However, it is necessary 391 to minimize experimental effort without compromising the quality of the research, at the 392 same time analytical results should be maximized. The schematic representation of the 393 design of experiments establishment process is shown in Fig. 3.3. Design of experiments 394 (DoE) is a systematic, efficient tool used for optimization and development of processes 395 or products. The classical approach to any test requires large number of experiments since 396 it is related to one-factor-at-a-time approach [234]. DoE methods allow to evaluate the 397 performance of product or quality of the process with only limited number of experiments 398 [235].

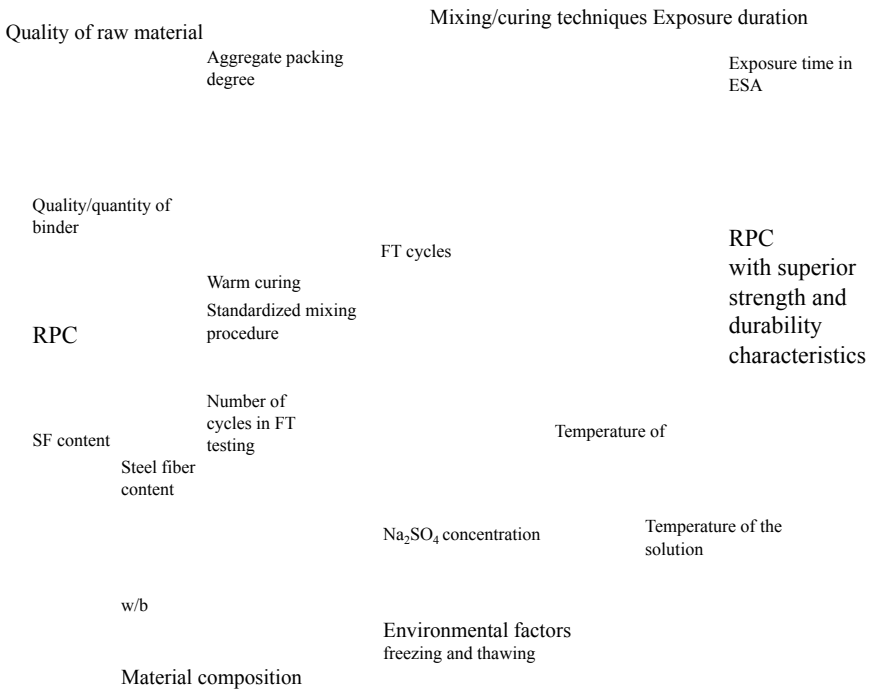

399

400 Fig. 3.3. RPC development process.

401 Fig. 3.3 shows that there are number of input variables such as quality of raw 402 material, mixing and curing techniques, material composition, environmental factors and 403 exposure duration that influence the output. The quantitative relationship between the 404 input variables and output signal can be determined with mathematical model, which will 405 numerically characterize the magnitude of impact of each variable [236].

406 3.3.1 Fractional factorial method

The Fractional Factorial Design (FFD) is a type of DoE expressed in the form of X^{k-p} 407 , 408 where X – levels of factor, k – number of factors, and p – fractionation used. FFD is used 409 for screening of 3 to 7 factors in experimental design [235, 237]. The FFD is a reduced 410 type of Full Factorial Design which involves running all possible combinations of factor 411 settings [238]. Full factorial design is capable design technique; however, it is not used 412 in the study since it is associated with large number of experiments.

413 3.3.2 Response surface method

414 Response Surface Method (RSM) is a special statistic method of a single-variable and 415 orthogonal array design. It is used at later stages of the research when important factors 416 were identified. It can model the curvature of the relationship between input variables and 417 output signal in 3D space [239, 240]. Central composite design (CCD) factors were used 418 to study the strength of RPC. Eq. 3.26 represents the quadratic model of the target with 419 respect to variables:

$$\text{Eq. 3.26:}\quad y = \beta_{0,0} + \sum_{i=1}^{k} \beta_{i,i} x_i x_i + \sum_{i} \sum_{j} \beta_{i,j} x_i x_j + \varepsilon$$

420 $\{3.26\}$ 421 where, x_i and x_j – coded values of the variables, β – regression coefficient, k – the 422 number of factors in the study, y – predicted response, i – linear coefficient, j – quadratic 423 coefficient, and ε – random error. The variation of variables for the RPC mixture 424 proportion was designed by Minitab statistic software.

425 3.3.3 Taguchi method

426 Taguchi DoE method employs orthogonal arrays to produce the objective functions to 427 evaluate the influence of the factors on the response data [235, 241]. One of the important 428 characteristics of Taguchi DoE is the quality loss function [241, 242]. The loss is a 429 variation of functional results due to uncontrolled factors [242, 243]. There are three types 430 of targets. This study is using Taguchi's smaller-the-better quality loss function. It is a 431 non-negative measurable characteristic. The ideal target is "0" [243]. The quality loss 432 function is defined as given in Eq. 3.27 and 3.28:

$$L(y) = k(y - 0)^2 = k y^2 \quad 433$$

434 {3.27}

$$\text{ }\text{ } = \frac{\text{ }\text{ }(\text{ }\text{ })}{\text{ }\text{ }^2 = \text{ }\text{ }_0}$$

435 $_2$

Δ_0

436 {3.28}

437 where, *Y* – value of the quality characteristic (e.g. strength); *L(Y)* – loss in value per 438 product when quality is *Y*; *K* – proportionality constant which depends on limits of the 439 specimen; A_0 – average cost of adjustment with deviation of Δ_0.

440 Experiments are designed using Orthogonal Arrays (OAs) require minimal number 441 of experiments to obtain the desired information [244]. As an illustration, full factorial DoE with 4 factors at 3 levels requires 81 (3^4

442) runs by FFD, while for Taguchi DoE 443 number of runs is 9. Table 3.4 summarizes the Degrees of Freedom and Number of 444 Experiments required for L9 Orthogonal Array Taguchi DoE with 4 factors at 3 levels.

445 Table 3.4. Determination of number of experiments.

Parameters	Levels	DoF Equations	A	3	2	DoF=Levels-1	B	3	2
C	3	2	Number of Experiments	D	3	2 =Total DoF + 1	Total:	8	9

446 Minimum number of experiments required for desired setup is determined as 447 described in Table 3.4. Hence, 9 experiments are required for determination of optimum 448 quality of RPC. To simplify, we have 9 experiments for 4 factors with 3 levels as a 449 baseline 9 mixtures that can be run for different conditions and tested for different 450 qualities.

451 Orthogonal Array is a universal class of combinational arrangements that can be 452 used to conduct the experiments to determine the optimum mix of several factors that can 453 maximize the yield [242-244]. The concept of orthogonality is determined by Eq. 3.29. 454 $\sum \text{ }\text{ }_{\text{ }\text{ }}\text{ }\text{ }_{\text{ }\text{ }} = 0$ {3.29}

455 In Taguchi Method a set of balanced minimum number of experiments is provided 456 by orthogonal array, while Taguchi's Signal-to-Noise ratios (S/N) which are logarithmic 457 function of desired output serve as functions for optimization in data analysis [241-243]. 458 Balance of Taguchi Design is achieved by the fact that factors do not influence each 459 other during experiments; and each factor has an equal weight.

460 3.4 Experimental setup

461 This chapter describes different experimental setups used for proportioning and testing 462 RPC mixtures using materials described in section 3.1 to run the tests described in section 463 3.2 based on the DoE described in section 3.3. Absolute volume method was used for all 464 RPC mixture proportioning since allows to calculate required quantity of the material for 465 any given number of samples with high precision.

466 3.4.1 RSM based mixture proportioning

467 ASTM Type I Ordinary Portland cement and locally available SF with properties as given 468 in Table 3.1, and fine quartz sand with properties as given in Table 3.2 were used for 469 these experiments. Ordinary tap water and a liquid superplasticizer (SP) Master Glenium 470 ACE 430 were used for the RPC mixing. The mixing was done following the procedure 471 in Fig. 3.1. The main aim of these experiments was to optimize the mixture proportioning 472 of RPC without steel fibers for appropriate compressive strength under normal and warm 473 curing conditions. Minitab statistic software was used to proportion the mixtures of RPC 474 in accordance with variation of SF content and WB. Corresponding CCD values are given 475 in Table 3.6 while Table 3.7 presents the mixture proportioning of RPC mixtures designed 476 using CCD RSM.

477 Table 3.6.CCD RSM applied for RPC.

No.	Mixture ID	w/b	Coded values of w/b	SF	Coded values of SF
1	**0.18WB-20SF**	0.18	-1.41	20	0
2	0.1917WB-23.54SF	0.1917	-1	23.54	1
3	**0.22WB-25SF**	0.22	0	25	1.41
4	**0.22WB-20SF**	0.22	0	20	0
5	0.2483WB-23.54SF	0.2483	1	23.54	1
6	**0.26WB-20SF**	0.26	1.41	20	0
7	0.2483WB-16.46SF	0.2483	1	16.46	-1
8	**0.22WB-15SF**	0.22	0	15	-1.41

9 0.1917WB-16.46SF 0.1917 -1 16.46 -1
10 0.18WB-0SF 0.18 NA 0 NA
11 **0.22WB-0SF** 0.22 NA 0 NA
12 0.26WB-0SF 0.26 NA 0 NA

478 Table 3.7. Mixture proportioning of RPC designed by CCD RSM.

No.	Mixture ID	Cement [kg/m3]	SF [kg/m3]	Sand [kg/m3]	Water [kg/m3]	SP [%]
1	0.18WB-20SF	1000	200	903	216	2
2	0.1917WB-23.54SF	971	229	861	230	2.5
3	0.22WB-25SF	960	240	776	264	1.5
4	0.22WB-20SF	1000	200	788	264	1.5
5	0.2483WB-23.54SF	971	229	698	298	1.125
6	0.26WB-20SF	1000	200	673	312	1.5
7	0.2483WB-16.46SF	1030	170	716	298	1
8	0.22WB-15SF	1043	157	802	264	1.5
9	0.1917WB-16.46SF	1030	170	879	230	2.5
10	0.18WB-0SF	1200	0	967	216	1.5
11	0.22WB-0SF	1200	0	852	264	1
12	0.26WB-0SF	1200	0	737	312	0.5

479 As it can be observed from Tables 3.6 and 3.7, in addition to the 9 mixtures 480 required for the RSM (Mixtures 1 to 9), 3 “plain” concrete mixtures (mixtures without SF 481 addition) with different WB were included to identify the baseline for the RPC 482 characterization.

483 3.4.2 Partial factorial DoE mix proportioning

484 Properties of ASTM Type I ordinary Portland cement and densified SF which were 485 used as binders for RPC preparation are given in Table 3.1. Locally available fine quartz 486 river sands were also used. Its properties are given in Table 3.2. Master Glenium ACE 487 430 superplasticizer (SP) and ordinary tap water were used for RPC mixtures.

488 The mixture proportion of RPC is given in Table 3.8. The mixture design is based 489 on the partial factorial DoE and original CCD RSM design of experiments presented 490 earlier in the chapter. Total six RPC mixtures were prepared, number of characteristics 491 such as modulus of rupture, effect of warm curing and shrinkage of the mixtures were 492 tested in the initial phase of the experiments. Second part of the experiments involved 493 their exposure to

3 different Na_2SO_4 concentrations (0.35 M, 0.7 M, and 1.4 M). The 494 influence of mixture content on RPC properties and choosing the optimum RPC mixture 495 was done through changing one of the parameters..

496 Table 3.8. Mixture proportion of RPC.

No. Mixture ID w/b SF Cement Sand SP (% of cement by mass) (kg/m^3) (% of binder)
1 0.22WB-0SF 0.22 0 1000 903 2 2 0.22WB-15SF 0.22 15 1000 788 1.5 3 0.18WB-20SF 0.18 20 1000 673 1.5 4 0.22WB-20SF 0.22 20 1043 802 1.5 5 0.26WB-20SF 0.26 20 960 776 1.5 6 0.22WB-25SF 0.22 25 1200 852 1.0

497 Namely, at constant w/b = 0.22, mixtures with 0 (or plain RPC mixture without SF), 498 15, 20 and 25% SF (Mixes No. 1, 2, 4 and 6); and, at constant 20% SF content w/b = 0.18, 499 0.22, and 0.26 (Mixes No. 3, 4 and 5). The quantity of each mixture component was 500 determined by absolute volume method. A slight variation of SP dosage was required to 501 maintain the target flowability value.

502 3.4.3 Mixture proportioning for packing degree study

503 Absolute volume method was used for mixture proportioning of RPC mixtures to 504 optimize packing degree of fine aggregate. Cement and SF content, and w/b of the mixtures were held constant as: 1200 kg/m^3
505 , 20% of cement by mass and 0.20 506 correspondingly. Properties of each sand fraction determined by ASTM C128 and ASTM 507 C29 testing methods are given in Table 3.9.

508 Table 3.9. Properties of each sand fraction.

Classification Number 1* 2 3 4 Sieve Number, [#] 30 50 100 200 Size range, [mm] 0.6-1.18 0.3-0.6 0.15-0.3 0.075-0.15 Absorption Capacity (AC), [%] 3.2211 3.9669 4.0602 6.0109 Moisture Content (MC), [%] 0.0339 0.1778 0.1767 0.3151 Apparent Specific Gravity (G_a) 2.7211 2.8271 2.8298 2.9163 Dry Rodded Unit Weight (DRUW), [kg/m^3] 1586.65 1644.64 1602.65 1577.53 Eigenpacking Degree (φ) 0.5831 0.5817 0.5663 0.5409 *Since Sand 1 is not abundant in raw river sand (only 2.3% is retained on the sieve) it had been excluded from further study.

509 A total number of 10 RPC mixtures with various proportioning of sand fractions (5 510 mixtures for combinations of sand 4&3&2 and 5 mixtures for combinations of sand 3&2) 511 had been tested for workability and compressive strength as required by ASTM C1437 512 and ASTM C109 testing methods respectively.

513 3.4.4 Taguchi DoE mixture proportioning

514 The Taguchi design of experiments (DoE) method was used to determine the 515 optimal mixture with

516 beneficial characteristics against ESA. Four factors including 3 mixture design 517 parameters and 1 exposure condition, with 3 levels for each factor were chosen based on 518 several previous studies. Taguchi L9 orthogonal array method to evaluate the ESA and 519 F&T performance of RPC based on various characteristics. Mixture proportioning is 520 provided in Table 3.10.

521 Table 3.10. Mixture Proportioning of RPC mixtures.

No.	Mix ID	w/b	Cement	SF	Sand	Steel Fiber	SP, [% of binder]	[kg/m^3]
1	0-0.16-15-0.35	0.16	1043	157	1155	0	6	
2	0-0.20-20-1.05	0.20	1000	200	1002	0	3	
3	0-0.24-25-3.15	0.24	960	240	851	0	2.5	
4	1-0.16-20-3.15	0.16	1000	200	1139	10	6	
5	1-0.20-25-0.35	0.20	960	240	987	10	4.5	
6	1-0.24-15-1.05	0.24	1043	157	882	10	3	
7	2-0.16-25-1.05	0.16	960	240	1124	20	8	
8	2-0.20-15-3.15	0.20	1043	157	1019	20	4.5	
9	2-0.24-20-0.35	0.24	1000	200	866	20	3	

522 The baseline properties of given mixtures were identified by workability, air voids 523 and porosity, sorptivity and compressive strength tests.

524 Thus, to study the effect of different exposure conditions on ESA resistance of RPC, 525 samples from 9 base mixtures were exposed to cyclic (1 week in air, 1 week in solution) 526 and continuous exposure at normal temperature (20 ºC), and continuous exposure at 40 527 and 60 ºC. Workability, compressive strength, modulus of rupture, length, and mass 528 change, UPV and dielectric conductivity of these mixtures were tested at different age up 529 to 52-week exposure duration. Microstructural analysis by SEM observation and porosity 530 test was performed on samples after completing the testing.

531 In addition, to study the effect of FT resistance of RPC, samples from 9 base 532 mixtures were exposed to freezing and thawing cycles as identified in section 3.2.5. MoR 533 of unexposed samples was measured on bar samples as in accordance with ASTM C293. 534 Length, and mass change, and UPV of bar samples was measured up to 300 cycles 535 followed by MoR test.

4. Mixture proportion and characterization of RPC

As a newly emerging material UHPC is suggested to be used in number of various applications starting from bridge decks to pile foundation systems with incorporated energy storage. This part of the research focuses on characterization of RPC mixtures without steel fibers in terms of their strength, optimizing the packing degree of fine aggregate to achieve improved material properties and small study of its ESA durability. Hence, results obtained in this part of the research were used to develop experimental program and design of experiments for the main study and helped to understand the basic patterns in RPC performance and its dependance on mixture design characteristics and their variation.

4.1 Optimization of RPC mixture design by response surface method

Performance of RPC depends on number of factors, and especially on its mixture proportioning and curing regime. This study focuses on the influence of variation of w/b, SF, and impact of normal and warm curing on RPC fresh and hardened properties. Fresh properties of interest include relative flowability, penetration resistance and setting time, while hardened properties include drying shrinkage, compressive and flexural strength.

Properties of binder materials and aggregates used for the RPC mixing in this set of experiments are provided in Tables 3.1 and 3.2. Section 3.1.3 describes supplementary materials used for RPC mixing, while the mixing procedure and sample preparation are described in Section 3.1.4. Mixing procedure is illustrated in Fig. 3.1 as well.

The details of RSM based mixture proportion can be found in Section 3.4.1. Mixture proportioning of 12 mixtures studied in this set of experiments is given in Tables 3.6 and 3.7.

Table 4.1 summarizes test methods and standards used in this part of the study.

Table 4.1. Experimental setup for RPC mixture optimization.

Experiment	Test method	Reference	Section
Flow table test	ASTM C1437	227	3.2.2
Setting time and penetration resistance	ASTM C403	228	3.2.2
Compressive strength	ASTM C109	234	3.2.4
Modulus of rupture	ASTM C293	236	3.2.4
Density, absorption, and voids	ASTM C642	239	3.2.3

54

24 Table 4.1. Experimental setup for RPC mixture optimization (cont.). Experiment Test method Reference Section

Drying shrinkage ASTM 157, ASTM C490 231, 232 3.2.3

25

26 4.1.1 Fresh properties of RPC

27 *Flowability of RPC*

28 Relatively high amount of SF added into RPC mixtures together with their low w/b make 29 workability one of the most important issues for consideration. The results of the flow table 30 test are provided in Table 4.2.

31 Table 4.2. Flowability of RPC mixtures.

No.	Mixture ID	Before dropping		After dropping		Γ_m
		d_1^0(mm)	d_2^0(mm)	d_1(mm)	d_2(mm)	
1	**0.18WB-20SF**	**110**	**110**	**150**	**150**	**1.25**
2	0.1917WB-23.54SF	100	107	195	200	2.90
3	**0.22WB-25SF**	**105**	**100**	**165**	**165**	**1.72**
4	**0.22WB-20SF**	**125**	**120**	**205**	**200**	**3.10**
5	0.2483WB-23.54SF	115	115	200	190	2.80
6	**0.26WB-20SF**	**120**	**125**	**250**	**250**	**5.25**
7	0.2483WB-16.46SF	110	110	150	155	1.33
8	**0.22WB-15SF**	**120**	**125**	**210**	**205**	**3.30**
9	0.1917WB-16.46SF	110	110	175	165	1.89
10	0.18WB-0SF	100	105	130	135	0.76
11	**0.22WB-0SF**	**100**	**100**	**160**	**165**	**1.64**
12	0.26WB-0SF	100	100	165	160	1.64

32 Results of the flow table tests show that all RPC mixtures tested (except Mix

33 0.18WB-0SF) had acceptable workability with flow diameter after dropping being 200±50

34 mm. This range ensures comfortable concrete handling and placing. 35 Flowability of RPC mixtures, Γ_m, is calculated using Eq. 3.8. Fig. 4.1 presents 36 relative flowability of six key mixtures.

Relative flowability

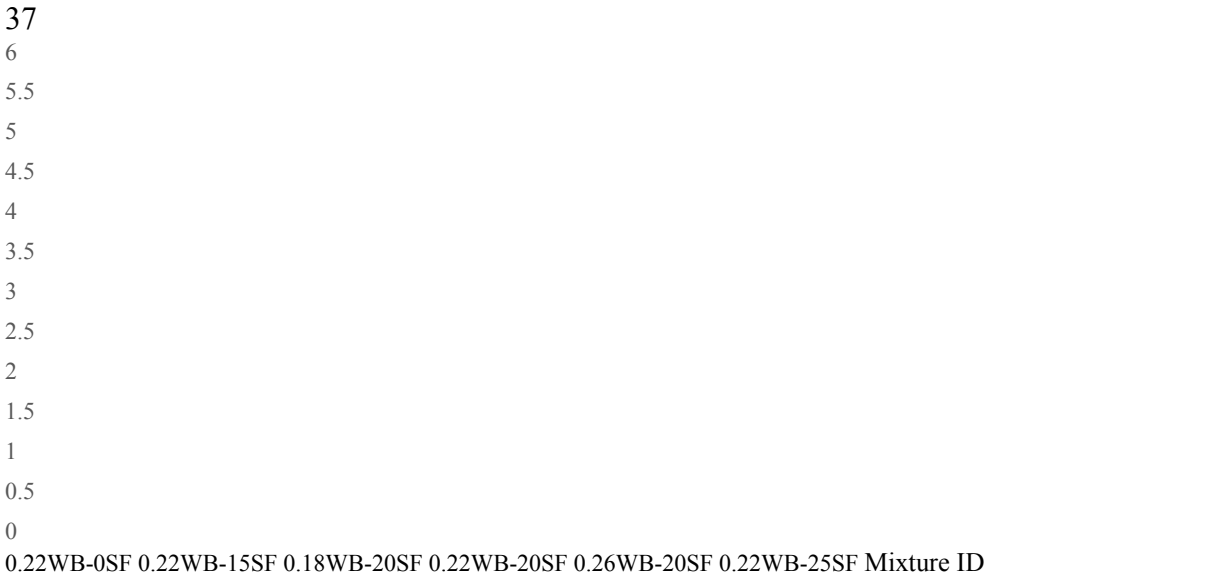

38 Fig. 4.1. Relative flowability of six key mixtures.

39 According to Fig. 4.1, increasing SF content tends decrease relative flowability of 40 RPC mixtures, while increasing w/b increases the value. It should be noted that relative 41 flowability of plain RPC mixture (mixture without SF addition) is considerably smaller 42 compared to other mixtures. Since all RPC mixtures had the same SP dosage, the reduction 43 of relative flowability that results from increase of SF content is possibly due to high specific 44 surface area of SF particles that lead to increased water demand of RPC mixtures with high 45 SF content. In addition, increasing w/b results in expected increase of relative flowability. 46 However, it can have a negative effect on other RPC properties. Furthermore, increasing 47 workability above a certain level result in difficulties in handling, placing, and setting of RPC 48 mixtures.

49 *Penetration Resistance and Setting Time*

50 Fig. 4.2 provides penetration resistance of six key mixtures obtained in ASTM C403 51 test [223]. Fig. 4.2 (a) shows the influence of changing SF content at constant w/b on 52 penetration resistance of RPC mixtures. Accordingly, decreasing SF content, in general, 53 tends to increase the time elapsed before the final set. In addition, plain concrete mixture with 54 0% SF dosage had faster setting compared to RPC mixtures which is probably attributed

by 55 the low SP dosage used for this mixture.

56

(a) SF=0% SF=15% SF=20% SF=25%

(b) w/b=0.18 w/b=0.22 w/b=0.26

56

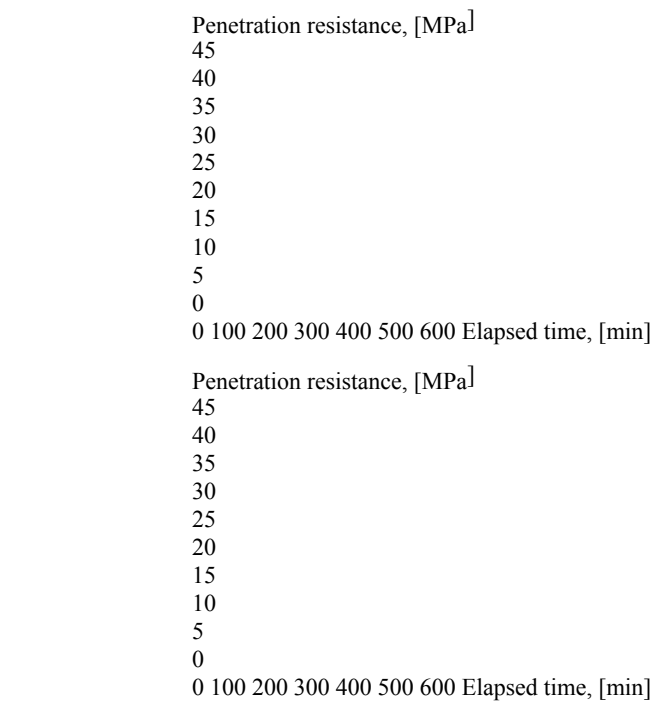

57 Fig. 4.2. Penetration resistance of RPC: (a) effect of SF content; (b) effect of w/b.

58 Based on Fig. 4.2 (b), where the influence of changing w/b at constant SF content 59 on penetration resistance of RPC mixtures is shown, it is possible to argue that increasing 60 w/b tends to significantly increase the time of setting in RPC mixtures. Since SP dosage was 61 kept unchanged for all mixtures, the change is most likely to be attributed by w/b of RPC 62 mixtures.

63 ASTM C403 sets standard values for the initial set and final set as the time elapsed 64 before reaching 3.44 MPa and 27.6 MPa penetration resistance respectively. Fig. 4.3 65 summarizes initial and final set times of six key RPC mixtures.

(a) SF=0 SF=15 SF=20 SF=25
(b) w/b=0.18 w/b=0.22 w/b=0.26

Setting time, [min]
66
500
400
300
200
100
0
Initial set Final set

Setting time, [min]
600
500
400
300
200
100
0
Initial set Final set

67 Fig. 4.3. Setting time of RPC: (a) effect of SF content; (b) effect of w/b.

68 Fig. 4.3 (a) indicates that plain concrete mixture with 0% SF content has 69 significantly lower initial and final set time compared to RPC mixtures. Hence, addition of 70 SF tends to increase the set time in RPC. However, Fig. 4.3 (a) shows that both initial and 71 final setting time decrease when SF content is increased at constant w/b. On the other hand,

72 Fig. 4.3 (b) shows that increasing w/b at constant SF content results in the increase of both 73 initial and final set time.

Setting time, [min]
600 500 400

Initial set Final set SF=0

y = 25.3x + 407.8 R² = 0.8372

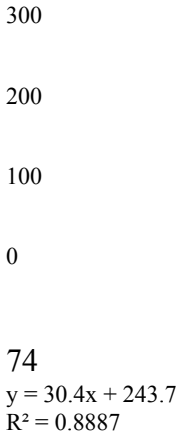

75 Fig. 4.4. Relative flowability vs. setting time of RPC mixtures.

76 Fig. 4.4 summarizes the relationship between the relative flowability and setting 77 time of RPC mixtures. Accordingly, both initial and final set time are linearly dependent on relative flowability of RPC mixtures. Equations of linear fit has relatively high R^2 78 values for 79 both initial and final set data. However, it should be noted that relative flowability and set 80 times of plain concrete mixture with 0% SF content was excluded from the linear fit, since it 81 had negative influence on the quality of linear estimation.

82 4.1.2 Hardened properties of RPC

83 *Compressive strength development of RPC*

84 Compressive strength development and porosity of RPC mixtures is presented in Table 4.3. 85 Table 4.3 shows that RPC studied RPC mixtures have relatively high compressive strength 86 values, their compressive strength tends to increase with increase of curing period. Majority 87 of the mixtures showed about 1.5-2 times increase of compressive strength between 1-day

88 and 28-day curing period. Typical value of compressive strength of RPC mixtures studied is 89 about 80 MPa at 28-days.

90 On the other hand, Table 4.3 shows that porosity of most RPC mixtures tends to 91 decrease with increase of curing period. Decrease of porosity of RPC mixtures is related to 92 continuous hydration and consequent microstructural refinement. Porosity of RPC mixtures 93 is related to its strength and durability. Thus, smaller porosity values indicate strong concrete 94 with continuous microstructure. As an illustration, mixture 0.1917WB-16.46SF has a 95 minimal porosity pf 3.59 % and maximal 28-day compressive strength of 90.33 MPa, while 96 mixture 0.26WB-20SF with the highest porosity value of 15.05% has one of the lowest 28- 97 day compressive strength values which is about 65.59 MPa.

98 Table 4.3. Compressive strength and porosity of RPC mixtures.

Mixture ID	Compressive strength, [MPa]							Porosit [%
	1-day	3-day	7-day	14-day	28-day	56-day	7-day	28-day
0.18WB-20SF	**44.23**	**41.10**	**67.05**	**74.14**	**79.65**	**82.15**	**3.84**	**4.14**
0.1917WB 23.54SF	37.72	72.70	83.65	66.17	73.38	82.92	5.27	5.77
0.22WB-25SF	**38.25**	**54.16**	**69.04**	**78.49**	**76.75**	**79.27**	**6.72**	**6.66**
0.22WB-20SF	**49.33**	**63.17**	**84.52**	**83.77**	**86.10**	**85.46**	**5.60**	**5.27**
0.2483WB 23.54SF	27.91	52.01	66.70	68.81	83.15	69.80	9.18	7.43
0.26WB-20SF	**30.92**	**46.80**	**62.31**	**65.59**	**70.31**	**90.05**	**12.95**	**15.05**
0.2483WB 16.46SF	36.99	62.70	68.01	69.73	70.43	76.55	8.43	8.77
0.22WB-15SF	**33.57**	**50.23**	**56.57**	**66.15**	**76.61**	**71.71**	**9.24**	**8.65**
0.1917WB 16.46SF	42.88	54.67	60.58	68.99	90.33	84.20	10.15	5.58
0.18WB-0SF	60.13	52.86	58.63	68.22	82.70	80.56	11.74	7.27
0.22WB-0SF	**40.25**	**53.23**	**65.54**	**57.72**	**73.45**	**79.03**	**10.17**	**13.47**

0.26WB-0SF	33.41	45.23	55.83	49.42	64.93	64.48	14.77	16.20

No. 56-day **1 5.28** 25.44

3 5.40 4 4.04

57.98 **6 10.80** 77.13 **8 11.34** 93.59

10 2.95 **11 8.61** 12 9.60 99 Both SF content and w/b have significant influence on compressive strength and

100 porosity of RPC mixtures. In general, compressive strength of concrete is expected to 101 increase with increasing curing time since it is assumed that concrete is undergoing 102 continuous hydration processes. Nevertheless, compressive strength decrease is observed 103 between 28-day and 56-day measurements for mixtures 0.1917WB-23.54SF, 0.22WB-25SF 104 and 0.22WB-15SF. Since porosities of these mixtures at 56-day were considerably higher

59

105 than at 28-day it is possible that hydration processes have considerably slowed down by 56- 106 day, and lead to formation of porous microstructure, which in turn resulted in the decrease of 107 compressive strength.

108 *Effect of SF content and curing temperature on compressive and flexural strength* 109 *of RPC.*

110 Fig. 4.5 summarizes the effect of changing SF content on compressive strength of 111 RPC mixtures after normal and warm temperature curing. Compressive strength of RPC 112 mixtures tends to increase with increase of curing period. However, the most significant 113 increase is observed between 1-day and 7-day measurements indicating that the initial 114 hydration processes are more likely to slow down by that period. Furthermore, Fig. 4.5 (a) 115 shows that compressive strength of RPC mixtures tends to gradually increase throughout the 116 measurement period at normal temperature curing. In contrast, Fig. 4.5 (b) shows that only 117 slight increase of compressive strength is observed for warm cured mixtures. Hence, warm 118 curing is more likely to facilitate early age strength in RPC rather than improving it long term 119 strength characteristics.

(a) SF=15 SF=20 SF=25
(b) SF=15 SF=20 SF=25

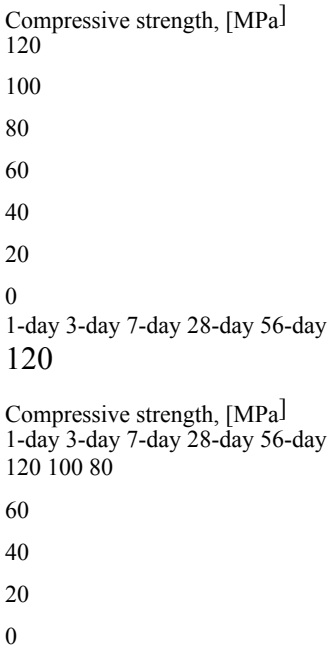

121 Fig. 4.5. Effect of SF content on compressive strength of RPC: (a) 23±2 °C; (b) 40±2 °C.

122 As it can be observed form Fig. 4.5 warm temperature curing tends to slightly 123 increase the compressive strength of RPC mixtures. Regardless of curing temperature, 124 increasing SF content from 15% to 20% increases the compressive strength of RPC. 125 However, when SF content is increased further to 25% compressive strength of RPC 126 decreases. Hence, addition of SF improves compressive strength of RPC up to a certain 127 optimum value, and further addition of SF does not result in compressive strength gain. It is

128 suggested that optimal amount of SF ensures strength of RPC through two mechanisms: 129 namely, pozzolanic reaction and filler effect. Hence, improvement of ITZ in concrete through 130 addition of SF results in even distribution of stresses. However, addition of excess SF can 131 lead to an excess of silicates compared to CH. Thus, pozzolanic reaction cannot occur, and 132 CSH lattices are not formed. In that case, excess SF acts simply as a filler resulting in the 133 decrease of compressive strength.

134 Fig. 4.6 shows 28-day flexural strength of RPC. Fig. 4.6 (a) shows that flexural 135 strength of normal cured RPC mixtures follows the same trends as compressive strength. 136 Thus, increasing SF content from 15% to 20% tends to increase flexural strength. However, 137 further increase from 20% to 25% results in the decrease of compressive strength.

(a) SF=15 SF=20 SF=25
(b) SF=15 SF=20 SF=25

Flexural strength, [MPa]
138
30
25
20
15
10
5
0
Normal curing

Flexural strength, [MPa]
30
25
20
15
10
5
0
Warm curing

139 Fig. 4.6. Effect of SF content on flexural strength of RPC: (a) 23±2 °C; (b) 40±2 °C.

140 Fig. 4.6 (b) shows that flexural strength of warm cured RPC mixtures tends to 141 decrease when SF content is increased from 15% to 20% and increase slightly when it is 142 increased further to 25%. It is argued that flexural strength of concrete typically depends on 143 porosity to density ratio (P/D). Thus, mixtures with low P/D tend to have higher flexural 144 strength. Table 4.4 summarizes porosity, density, and P/D of 6 key mixtures.

145 Table 4.4. Density, porosity, and P/D of six key RPC mixtures.

No.	Mixture ID	Density, [kg/m3] Normal curing	Density, [kg/m3] Warm Curing	Porosity, [%] Normal curing	Porosity, [%] Warm Curing	P/D Normal curing	P/D Warm Curing
1	0.22WB-0SF	2.26	2.24	13.47	13.1	5.96	5.85
2	0.22WB-15SF	2.21	2.24	8.65	8.16	3.91	3.64
3	0.18WB-20SF	2.23	2.19	4.14	5.75	1.86	2.63